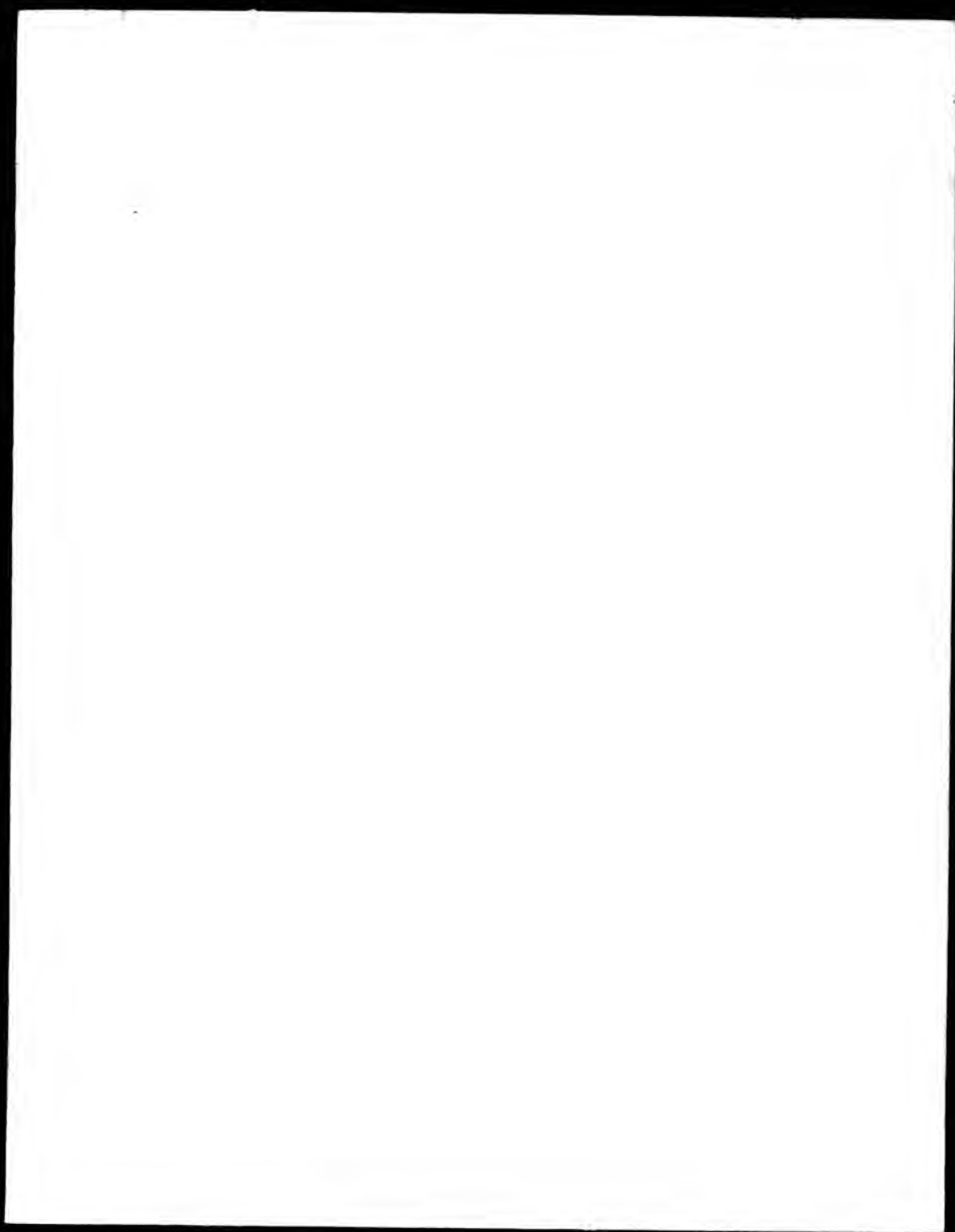
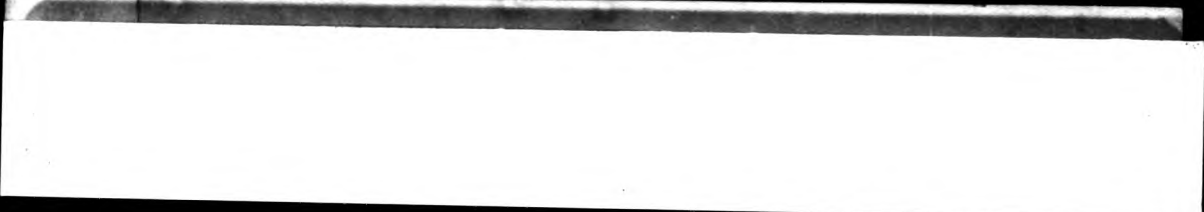
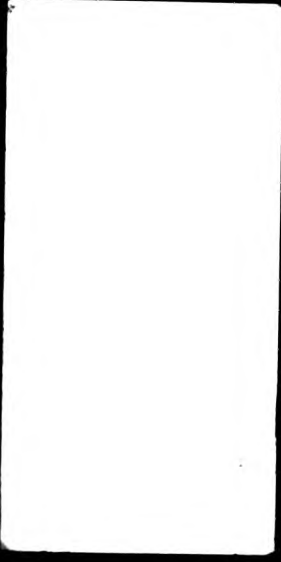


**This PDF was created from the British Library's microfilm copy of the original thesis. As such the images are greyscale and no colour was captured.**

**Due to the scanning process, an area greater than the page area is recorded and extraneous details can be captured.**

**This is the best available copy**

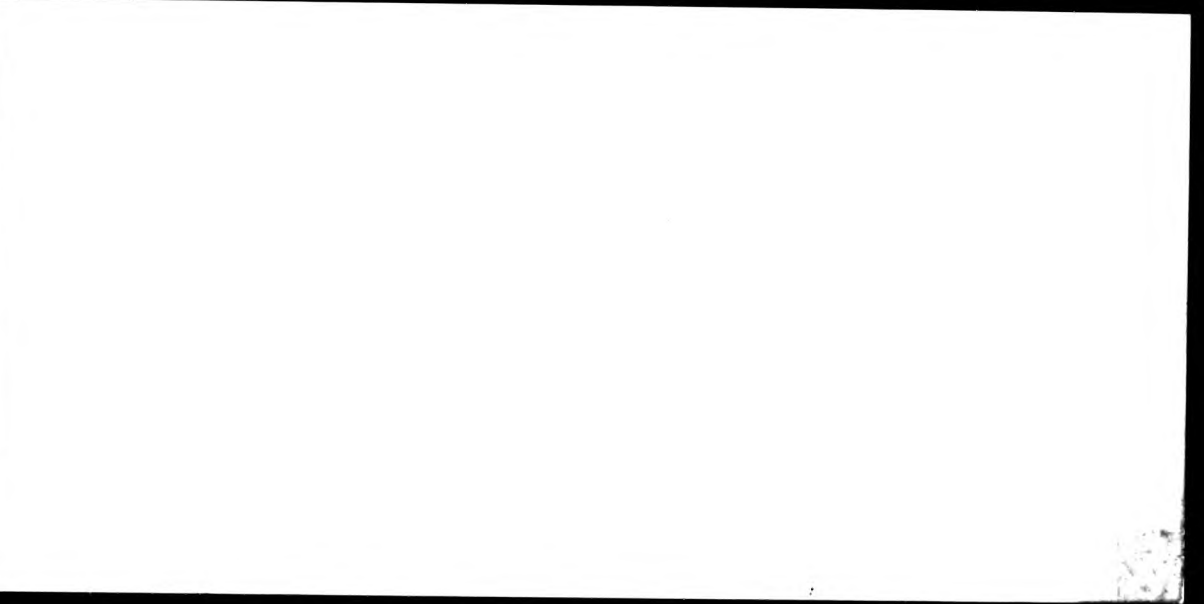


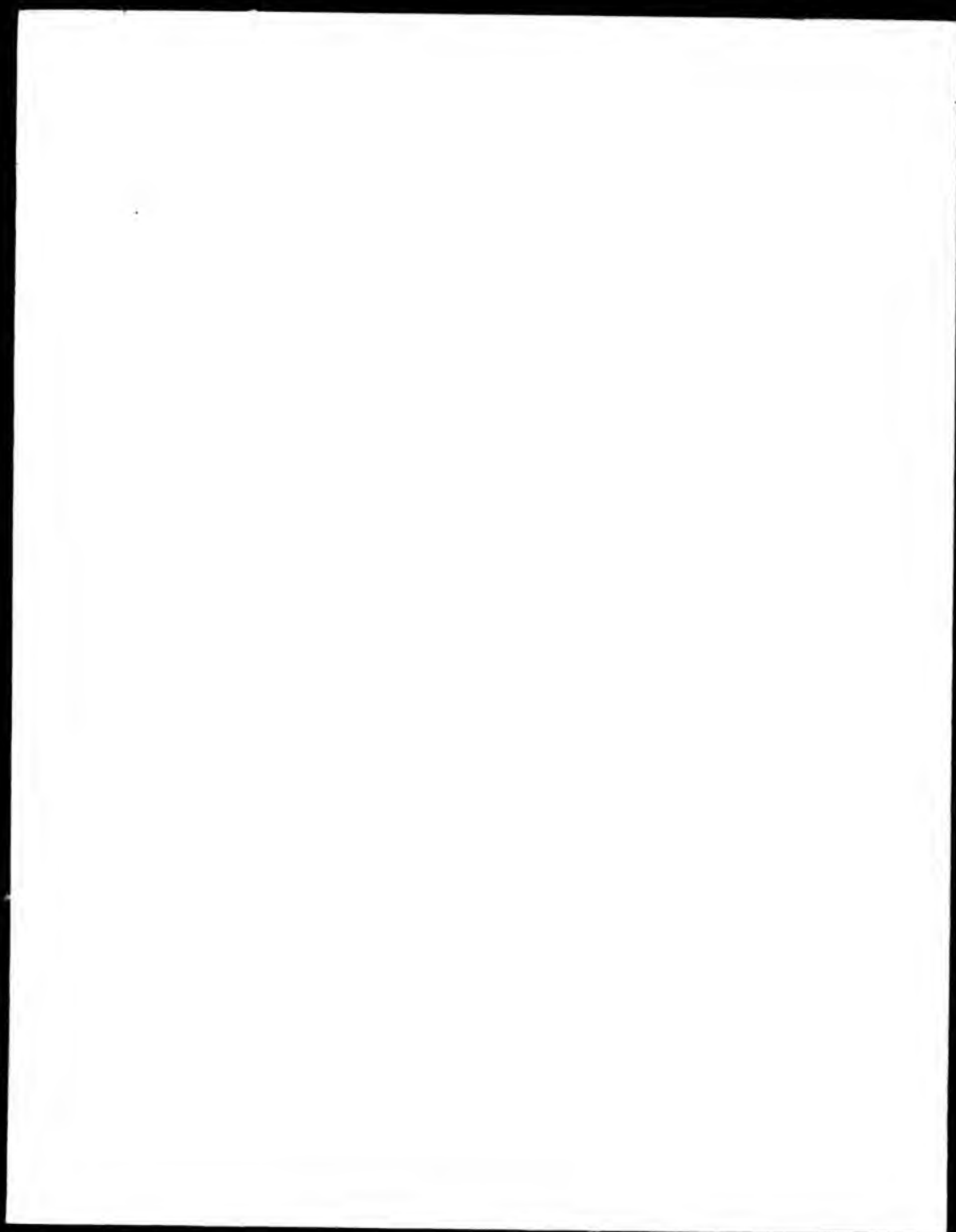


**DX**



<b>8</b>	<b>5</b>	<b>6</b>	<b>6</b>	<b>3</b>
----------	----------	----------	----------	----------





THE BRITISH LIBRARY DOCUMENT SUPPLY CENTRE

TITLE ..... OPTICAL PROPERTIES OF CONCENTRATED DISPERSIONS

AUTHOR ..... PETER J MOLLOY

INSTITUTION  
and DATE ..... CITY OF LONDON POLYTECHNIC  
1986

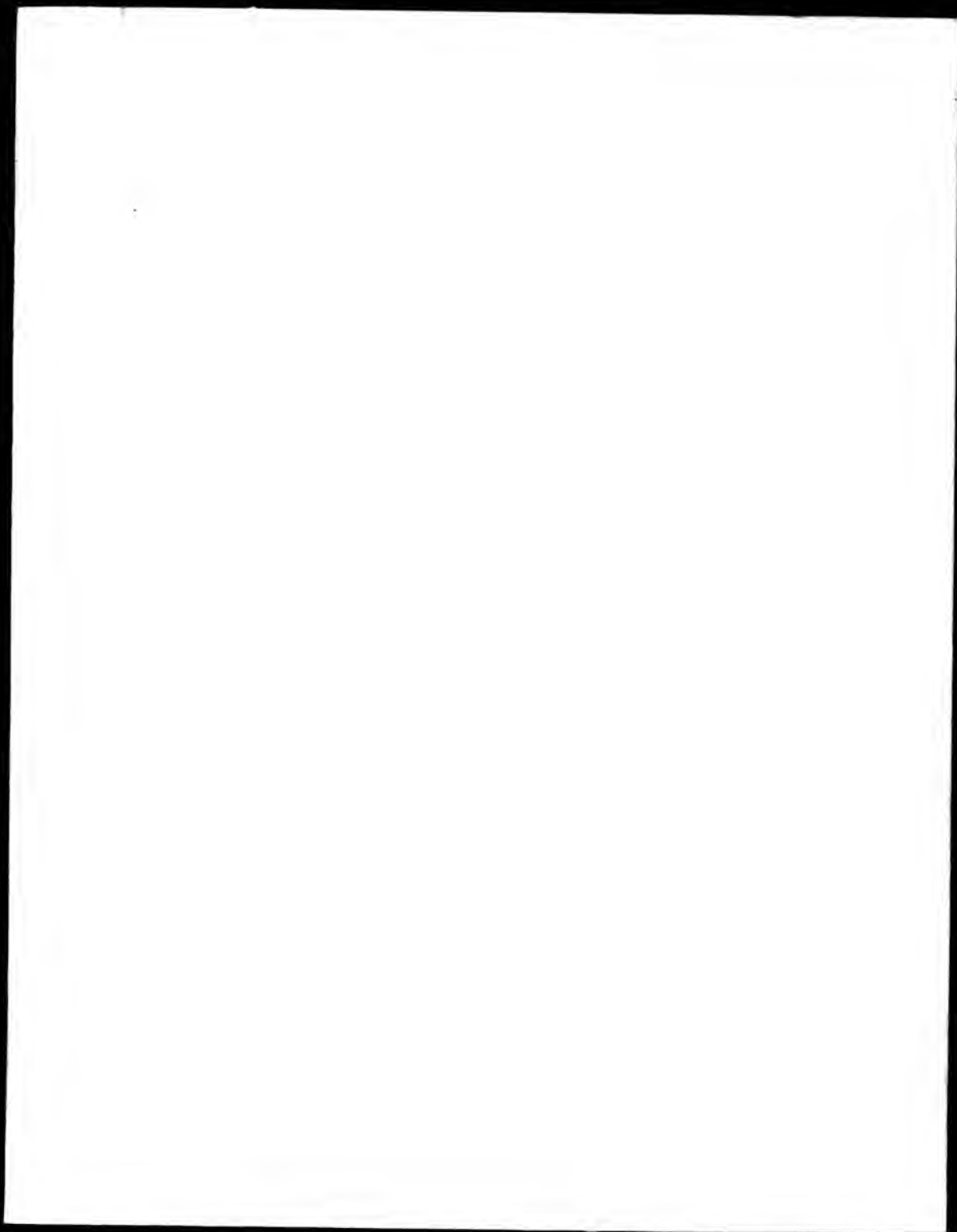
Attention is drawn to the fact that the copyright of this thesis rests with its author.

This copy of the thesis has been supplied on condition that anyone who consults it is understood to recognise that its copyright rests with its author and that no information derived from it may be published without the author's prior written consent.

1	1	2	3	4	5	6
cms						

THE BRITISH LIBRARY  
DOCUMENT SUPPLY CENTRE  
Boston Spa, Wetherby  
West Yorkshire  
United Kingdom

REDUCTION X ..... 21



OPTICAL PROPERTIES OF CONCENTRATED DISPERSIONS

BY PETER J. MOLLOY

A thesis submitted for the degree of  
Doctor of Philosophy in partial fulfilment of  
the requirement of the Council for National  
Academic Awards

Physics Department,  
City of London Polytechnic,  
31 Jewry Street,  
London EC3N 2EY.

In collaboration with English China Clays  
International.

December 1986

OPTICAL PROPERTIES OF CONCENTRATED DISPERSIONS

Peter J. Molloy

ABSTRACT

Apparatus and methods have been developed to measure the diffuse transmittance  $T$  and reflectance  $R$  of multiple scattering, concentrated, colloidal dispersions. The variation of  $R$  and  $T$  with pathlength, wavelength, and concentration has been investigated for non-spherical particles in concentrated dispersions, over a range of pH and surfactant concentrations.

Measurements of diffuse transmittance and reflectance required large corrections to be made for the presence of any specular interfaces i.e. windows.

These corrections were minimised by developing a bifurcated fibre optic bundle reflectance method, which allowed  $R$  and  $T$  to be measured at volume fractions up to at least 0.3.

Using magnetic, acoustic and shear fields to align the non-spherical kaolinite particles changes in  $R$  and  $T$  were measured at volume fractions upto 0.3.

The amplitude of the changes and the relaxation of the changes induced by the applied fields were measured. The amplitude of the change was found to vary strongly with pH and surfactant concentration. For any particular face diameter platelet, the amplitude of the change followed closely the flocculation process, and was sensitive to the mode of particle-particle aggregation, e.g. face-face, or face-edge. The amount of surfactant per unit mass of kaolinite required to stabilise dispersions is found to vary with particle size and concentration.

This showed that information about particle orientation can be obtained through multiple scattering systems when subjected to an aligning field.

Kubelka-Munk two flux theory was used to relate  $R$  and  $T$  to the diffuse flux scattering parameter  $S$ . A simple theory was developed relating  $S$  to the size shape and orientation of the non-spherical particles, hence allowing the particle orientation to be determined for any aligning field

The insight into particle behaviour given by the optical method is superior to that given by rheology alone, which does not provide an unambiguous measure of the mode of particle alignment.



Acknowledgements

I would like to thank my supervisor, Dr. G.H. Meeten, for his help and encouragement throughout this work. I would also like to thank Mr. Wiffen for his practical help and advice. Finally I would like to thank the City of London Polytechnic for a Research Assistantship whilst carrying out this work.

THANKS

CONTENTS

CHAPTER	PAGE
1) INTRODUCTION	1
2) MEASUREMENT OF THE SCATTERING PARAMETER S IN CONCENTRATED DISPERSIONS	26
3) EXPERIMENTAL INVESTIGATION OF MAGNETIC ORIENTATION	45
4) ULTRASONIC ORIENTATION	69
5) SHEAR-INDUCED ORIENTATION	83
6) CONCLUSION	108
7) REFERENCES	112

## CHAPTER 1

### Introduction

The usefulness of optical techniques to characterise suspensions of colloidal particles has long been demonstrated. These techniques have been confined almost completely to dilute dispersions where optical interactions between particles can be neglected due to their large separation, and consequently the results of experiments can be interpreted reliably using single scattering theory. In concentrated dispersions, where multiple scattering is dominant, investigative optical techniques have been mostly applied to the diffuse scattering of spherical particles where radiative transfer theory equations can be approximately solved, or to dispersions where there is long range order and Bragg-type coherent scattering is dominant.

Both areas have been recently reviewed[1]. This thesis presents results for the diffuse scattering from non-spherical particles.

When a light beam is transmitted through a dispersion of particles, some of the energy is lost from the primary beam due to scattering and absorption by the particles (neglecting scattering and absorption by the continuous media). By the law of conservation of energy the extinction cross-section per particle  $C_{ex}$  is the sum of the absorption and scattering cross-sections i.e.

$$C_{ex} = C_{ab} + C_{sc} \quad (1.1)$$

Providing there is no multiple scattering i.e. light

scattered by one particle does not then interact with another before emerging from the sample, the coherent transmittance (T) can be characterised by the Beer-Lambert law, which results from the assumption that equal path-lengths of the sample remove (by scattering or by absorption) equal fractions of the power of the incident beam. The Beer-Lambert law can be written;

$$T = \exp(-N C_{ex} d), \quad (1.2)$$

where N is the number of scatterers per unit volume, and d is the path length.

This can also be written in terms of the concentration as,

$$T = \exp(-\bar{\tau} c d), \quad (1.3)$$

where  $\bar{\tau}$  is the specific turbidity and c the concentration.

In order to make turbidity measurements within the Beer-Lambert region, of large particles with a large  $C_{ex}$  it is necessary to keep N small to avoid multiple scattering. It is then found experimentally that the transmitted beam amplitude fluctuates due to the temporal variations in the mean number of scatterers within the illuminated volume(2).

These variations in the number of scatterers follow the Poisson distribution. For non-spherical particles e.g. kaolinite there are also likely to be temporal variations in  $C_{ex}$  due to orientation fluctuations.

There are therefore two kinds of fluctuations: one depending on the mean number of particles in the illuminated volume; and the other depending on the mean orientation. The frequency at which these variations take place depends on the particle size and shape i.e. the

rotational and translational diffusion constants[3]. If there is no coupling between these two then a frequency spectrum of the transmitted light should show two peaks characterising the distributions. For a polydisperse sample there is also a time dependency in the size distribution in the illuminated volume if sedimentation occurs.

In order to measure the signal fluctuations, (referred to here as the noise), the noise is first maximised by reducing the beam width and increasing the path length for the same optical thickness. Its frequency range can be increased by flowing the sample[4]. If the fluctuations are unwanted e.g. when mean turbidity measurements are required, the beam width is increased and the path length reduced for the same optical thickness. If the particles and the refractive index mismatch are large then the concentration must also be increased, however here the angle scattering criteria required by the Beer-Lambert law no longer hold (i.e. that the path length should be less than the mean free path of photons, for the concentration used). In this case theories of multiple scattering are needed.

There have been various theories put forward to predict the macroscopic properties of multiple-scattering dispersions. Of these the most practicable are the two and four flux theory, reviewed below.

### 1.1 Two Flux Theory

In 1931 Kubelka and Munk[5] proposed a theory based on a model of two diffuse fluxes one in the forward direction and the other in the backward direction. The theory was later revised by various authors into its present form. It has been found that this two-flux theory gives good agreement with experimental results if the illumination is diffuse and the surface of the medium is dull so that the light is diffusely scattered into and out of the medium. It should be noted here that most experimental work has been concerned with measurements of diffuse reflectance and not transmittance.

For a non-absorbing medium the Kubelka-Munk expression for the diffuse transmittance reduces to the simple form

$$T = \frac{1}{1+Sd} \quad (1.4)$$

where  $d$  is the path length and where  $S$  is an operationally defined scattering parameter and  $T$  is the diffuse transmittance. The diffuse reflectance  $R$  is given by,

$$R = \frac{Sd}{1+Sd} \quad (1.5)$$

This simple model requires that a thin parallel layer is illuminated with a completely diffuse incident flux, and does not incorporate the corrections necessary when the sample is not a solid block of material but is fluid and requires a vessel to contain it.

In the experiments to be described here a diffuse source

was not used. The incident flux was provided either by a broad and approximately parallel collimated beam or by a fibre optic bundle having an angular spread of about sixty degrees.

#### 1.2 Four Flux Theory

Mudgett and Richards[6] and Ishimaru[7] discuss normal illumination of a thin, parallel-sided sample by a parallel, collimated beam. The discussion is simplified if neither collimated nor diffuse beam reflectance is considered at the un-illuminated face. There are then two diffuse beams and one forward collimated beam. The collimated flux is continuously converted to the two diffuse fluxes as it propagates through the sample layer.

For a thin slice of sample,  $dz$ , a collimated and forward going beam of flux density  $I$  causes diffuse flux densities  $IS_1 dz$  in the  $+z$  direction and  $IS_2 dz$  in the  $-z$  direction. The two diffuse fluxes couple via a scattering parameter  $S$  as in the Kubelka-Munk theory. There is no transfer of diffuse to collimated flux.

Using this approach, the total transmittance, which is the diffuse plus the collimated transmittance is given by

$$T = \frac{S_2 S \exp(-S'z) + S + S_1}{S'(1 + S_2)} \quad (1.6)$$

Where  $S' = (S_1 + S_2)$ , and zero absorption has been assumed.

Comparing this result with those of radiative transfer theory given by Ishimaru for a collimated beam[7], which for the case of zero absorption gives,

$$T = \frac{1 + 0.25 (1 - \exp(-NC_{sca} z))}{1 + 0.75 NC_{sca} z (1 - \langle \cos \theta \rangle)} \quad (1.7)$$

we find that they are the same if

$$S = (3/4 - 3/4 \langle \cos \theta \rangle) NC_{\text{sc}} \quad (1.8)$$

$$S_1 = (1/2 + 3/4 \langle \cos \theta \rangle) NC_{\text{sc}} \quad (1.9)$$

$$S_2 = (1/2 - 3/4 \langle \cos \theta \rangle) NC_{\text{sc}} \quad (1.10)$$

Here  $\langle \cos \theta \rangle$  is the intensity weighted average cosine of the angles through which photons are scattered, i.e. a correction term for non-isotropic scatterers. This is

$$\text{given by [8]} \quad \langle \cos \theta \rangle = \frac{1}{C_{\text{sc}}} \int_0^{4\pi} \delta(\omega) \cos \theta \, d\omega \quad (1.11)$$

where  $\delta(\omega)$  is the scattered flux per unit solid angle. This shows that the  $S$  measured in a multiple scattering dispersion can be directly related to the single scattering  $S$  i.e.  $NC_{\text{sc}}$  by the factor  $\frac{3}{4}(1 - \langle \cos \theta \rangle)$ .

### 1.3 Two flux theory with boundary corrections

Although the four flux theories allow for non-diffuse illumination they do not take into account the effects of boundaries.

Consider a sample layer with perfectly matt back and front faces which is fronted and backed by two external surfaces  $F$  and  $B$  at  $z = 0$  and  $z = Z$ , respectively, as in figure 1.1.

Only diffuse flux will be considered for simplicity. Suppose the incident flux density on  $F$  is unity, the reflectance is  $R$  and the transmittance is  $T$ . The planes  $F$  and  $B$  have all the properties of real interfaces. Thus  $F$  as a window will have a reflectance corresponding to the air-window surface and the window-dispersion surface, and similarly for  $B$ . The reflectances of  $F$  or  $B$  will generally depend on the flux direction. Light entering the layer



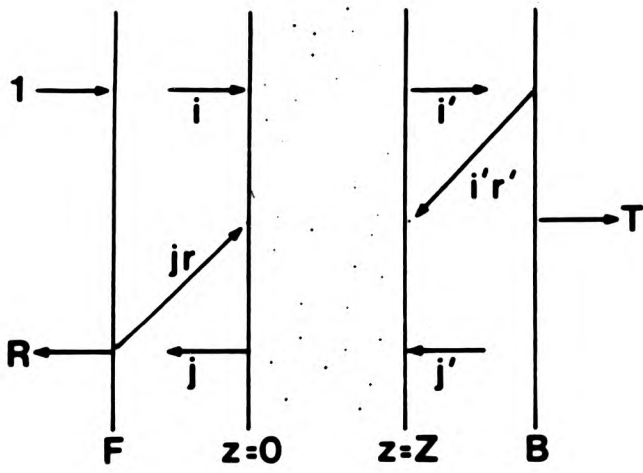


Figure 1.1 A perfectly matt surfaced sample of thickness  $Z$  fronted and backed by planes  $F$  and  $B$

will experience the external reflectances and transmittances  $\rho$  and  $\tau$  at F and  $\rho'$  and  $\tau'$  at B. Light leaving will experience the internal reflectances and transmittances  $r$  and  $t$  at F and  $r'$  and  $t'$  at B. Assuming that F is non-absorbing we have,

$$\rho + \tau = r + t = 1. \quad (1.12)$$

With the flux densities  $i, i', j, j'$  as shown in figure 1.1, it follows that

$$i' = iT_0 + j'R_0 \quad (1.13)$$

$$j = j'T_0 + iR_0 \quad (1.14)$$

for the bare layer of intrinsic transmittance  $T_0$  and reflectance  $R_0$  at the interfaces, the figure shows that,

$$i = \rho + jr, \quad (1.15)$$

$$j' = i'r, \quad (1.16)$$

$$R = \rho + jt, \quad (1.17)$$

$$T = i't'. \quad (1.18)$$

Elimination of  $i', i, j'$  and  $j$  from the above gives

$$R(T_0, R_0) = \rho + \frac{\tau t (R - r'(R_0^2 - T_0^2))}{(1 - R_0(r + r') + rr'(R_0^2 - T_0^2))} \quad (1.19)$$

and

$$T(T_0, R_0) = \frac{\tau t' T_0}{(1 - R_0(r + r') + rr'(R_0^2 - T_0^2))} \quad (1.20)$$

As  $R(T_0, R_0)$  and  $T(T_0, R_0)$  represent the measured properties it is seen that the boundary effects may be dominant.

For the case of a non-absorbing sample and using the two flux approximation we have

$$T(T_0, R_0) = \frac{A}{1 + BSz} \quad (1.21)$$

and

$$R(T_0, R_0) = \frac{A(Sz(1 - r') + r')}{1 + BSz} + \rho \quad (1.22)$$

where

$$A = \tau t / (1 - rr') \quad (1.23)$$

$$B = (1 + rr' - r - r') / (1 - rr') \quad (1.24)$$

For  $r = r' = 0.6$ ,  $\rho = 0.1$  and  $\epsilon = 0.9$  using Judd's values for internal reflectance(9) we have

$$A = 0.56$$

$$B = 0.25$$

giving

$$T = \frac{0.56}{(1+0.258z)}$$

and

$$R = 0.1 + \frac{0.2258z + 0.3375}{(1 + 0.258z)}$$

From the above it will be seen that the corrected transmittance has the same functional form as the intrinsic transmittance. However this is only true for completely diffuse incident flux. For the case of collimated incidence the constants used in the analysis above will become dependant on the angular distribution function of the intensity and will therefore become functions of the optical depth.

#### 1.4 Orientation phenomena

In this work magnetic, acoustic and shear fields have been used to orient non-spherical kaolinite particles in concentrated dispersions. Measurements of the reflectance or transmittance have been used to investigate the changes induced by this orientation in the properties of the dispersions. Acoustic orientation will be discussed in chapter 4.

### 1.5 Magnetic orientation.

The properties of kaolinite are discussed below. Magnetic impurities will be briefly discussed here, however for a fuller discussion reference should be made to Champion et al[10].

In the absence of iron contamination kaolinite would be expected to show diamagnetic properties. In general this is not the case, the magnetic properties exhibited by kaolinite are primarily a function of the iron associated with it, both as iron substituted in the lattice and as iron oxides associated with the surface. In kaolinite substitution occurs as  $Fe^{3+}$  for  $Al^{3+}$  in the octahedral lattice sites[11]. For low levels of iron ( $Fe_2O_3 < 0.5wt\%$ ) the paramagnetic susceptibility of kaolinite is proportional to the iron content but it is difficult to account for the magnitude of the paramagnetic susceptibility in terms of the  $Fe^{3+}$  content of the clay since  $Fe^{3+}$  has a symmetric wave function which can only produce small anisotropy. A much greater susceptibility is produced by the  $Fe^{2+}$  ion[12] but this ion only occurs at low levels in the lattice[11]. Several electron microscopic studies [13][14][15] have shown evidence for the presence of alpha hematite in the form of sub-micron particles attached to the surface of kaolinite. In particular the Mossbauer spectra of the alpha hematite on kaolinite strongly suggest that the fine particles are superparamagnetic at room temperature i.e. they consist of domains over which the electron spins are fully aligned. Between discrete superparamagnetic particles any

interactions must be long range such that the net magnetic moment is constrained to the longest dimension.

The magnitude of the observed mean mass paramagnetic susceptibility of kaolinite is given by Champion et al[10] as of the order of  $6 \times 10^{-9} \text{m}^3 \text{kg}^{-1}$  that is of the same order of magnitude as Aluminium and therefore field strengths of the order of Teslas are required to achieve complete orientation and dominate the effects of Brownian motion. However Champion et al[10] show that orientationally dependant properties can be measured with field strengths of the order of 0.1T. Field strengths of this magnitude can be obtained with a simple Helmholtz pair arrangement.

#### 1.6 Shear induced orientation

The motion of small particles suspended in shear flow has been studied both experimentally and theoretically for approximately 60 years.

The starting point for most of the recent theoretical work has been Jeffery's [16] solution of the Stokes equation for a small rigid spheroid suspended in a fluid undergoing laminar shear flow, showing that in the absence of body forces or couples, a spheroid will translate with the velocity of the undisturbed fluid, while its axis of revolution rotates in one of an infinite family of orbits. The instantaneous orientation of the particle is obtained from the integrated form of Jeffery's[16] equations giving

$$\tan \theta = \frac{Cr_p}{(\sin^2 \phi + r_p^2 \cos^2 \phi)^{1/2}} \quad (1.25)$$

$$\tan \phi = r_p \tan \left( \frac{2\pi t}{T} \right) \quad (1.26)$$

where  $r_p$  is the particle axis ratio. The spherical polar angles specify the orientation of the axis of revolution at a time  $t$  defined with respect to the fixed Cartesian co-ordinate system as shown in figure 1.2. Also shown are the velocity components  $U_i$

$$U_1 = U_2 = 0 \quad U_3 = GY$$

where  $G$  is the rate of shear. The influence of the initial orientation on the subsequent motion is expressed by the orbit constant  $C$ . According to these equations, the axis of revolution of a particle rotates about the  $z$  (vorticity) axis with a period  $T$  given by

$$T = \frac{2\pi}{G} \left( r_p + \frac{1}{r_p} \right) \quad (1.27)$$

Mason [17] has shown that good agreement with Jeffery's [16] theory is observed for very dilute suspensions of large (50-300 $\mu$ m) rod and disc shaped particles if  $T$  is measured experimentally thus defining the equivalent spheroidal axis ratio and not the true axis ratio.

According to Jeffery's [16] analysis a particle will remain indefinitely in any given orbit, leading to the possible assumption that the distribution of orbits is completely determined by the initial particle orientation distribution.

Jeffery's theory however, neglects the effects of: Brownian motion; fluid and particle inertia; and particle-particle interactions. It is thought [18] that these effects give rise to changes in the orbit of a particle eventually leading to a steady state distribution of orbits [18] independent of the initial distribution of orientations. This steady state distribution is therefore dependent on

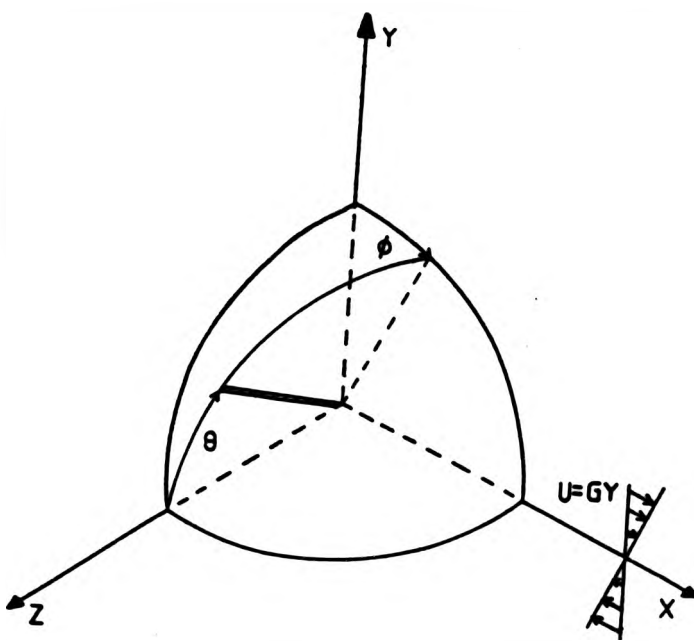


Figure 1.2 Coordinate system for describing the orientation of an axisymmetric particle. The spherical polar angles of the axis of revolution are shown relative to the shear flow  $GY$

the effects listed above and the shear rate, however in this work the particle Reynolds number was sufficiently small to discount the effect of inertia and the observed re-orientation on the cessation of shear is thought to be dominated by the effects of Brownian motion and particle-particle interactions.

#### 1.7 Colloidal dispersions.

The properties of colloidal *particles* are largely determined by their surface properties. Their surfaces are generally electrically charged as a result of surface defects, contamination and the preferential adsorption of ions. In an electrolytic solution this charged surface develops a diffuse ionic cloud with an excess of oppositely charged ions in its vicinity, which balance the charge on its surface. This electric double layer was first considered by Helmholtz[19] and later theoretically by Gouy[20] and Chapman[21]. The double layer consists of two parts, a strongly bound layer of *counter* ions, opposite in charge to those on the surface (the solvating layer), and the rest of the ionic cloud which is mobile but occupies a finite volume around the particle. This is known as the diffuse double layer. When the particle moves it carries with it the solvating layer whose *upper* extent is the slip plane. The potential at the slip plane is defined as the zeta potential and is the potential effective in electrokinetic behaviour. The zeta potential is considered one of the most useful parameters in determining dispersion stability.



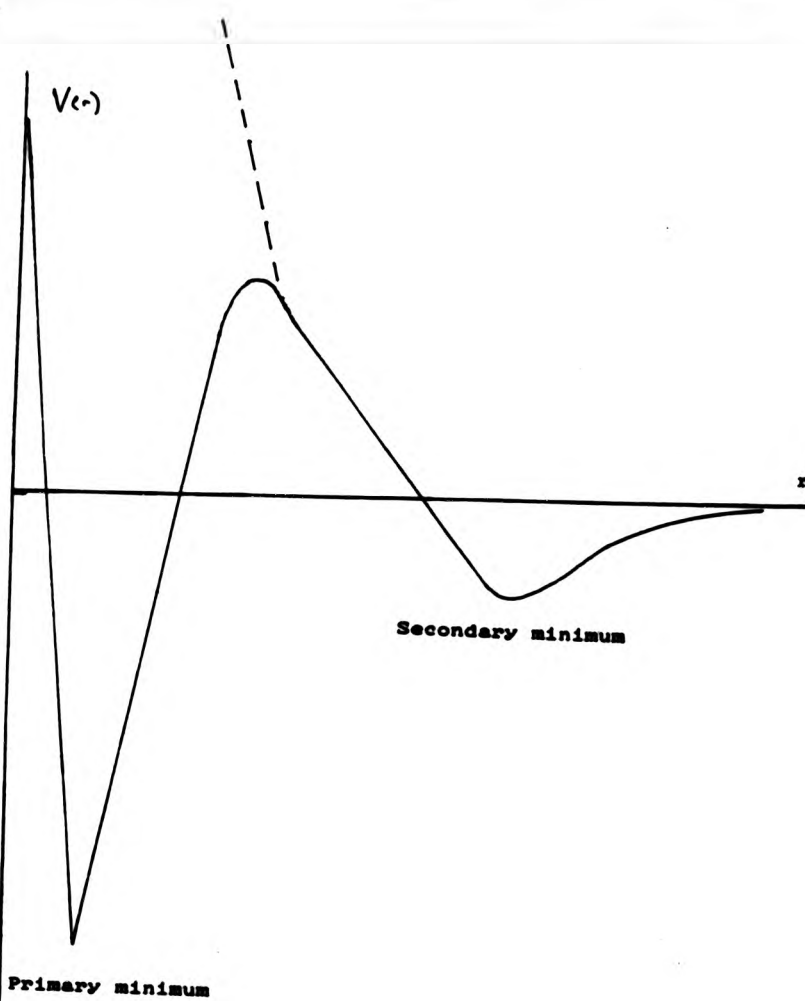


Figure 1.3 Interparticle potential energy as a function of separation  $r$

The dashed line represents the steric interaction due to adsorbed polymer chains.

The stability of a dispersion depends on the combination of the effects of Van der Waals attraction between particles and the repulsion between electric double layers. The proposition that these energies of repulsion and attraction are additive and that therefore the potential energy between particles could be obtained from their sum was put forward by Derjaguin and Landau[22] and Verwey and Overbeek[24]. This theory was later modified

to include the addition of a further term to account for Born repulsion, which is a very close range interaction due to the overlap of molecular orbitals. This forms the basis of the current theory of colloid stability.

Using the present theory a potential energy diagram can be sketched for a colloidal dispersion and has the form shown in figure 1.3. When two particles in such a dispersion approach each other they may become weakly bound in the secondary minimum or for a more energetic interaction they may become more strongly bound in the primary minimum. The relative probabilities of these two forms of aggregation depends on the height of the potential barrier and therefore the average interparticle separation.

The form of the curve shown in figure 1.3 is dependant on particle size as well as other properties of the dispersion e.g. concentration and the presence of adsorbed polymer films and the electrolyte concentration.

The presence of adsorbed polymer molecules around the particles leads to a structured layer. In order for the

particles to aggregate some perturbation of the conformations of the adsorbed chains, and displacement of solvent from the interfacial region into bulk is necessary.

This therefore contributes a further repulsive force to the interaction potential. This force is known as the steric interaction and can be maximised to produce semi-permanent stable dispersions[25]. For concentrated dispersions the situation is more complex requiring theories that can account for many body interactions[26][27].

All the present theories for both dilute and concentrated dispersions pertain to particles that have a ~~uniform~~ surface charge. In the case of kaolinite this condition is not satisfied as the charge on the particle edge is pH dependant (see below). Further discussion of theories of colloid stability for concentrated dispersions is therefore not useful. However Kline[28] has shown that the simple two body interaction potential shows reasonable qualitative agreement with observed rheological data for volume fractions up to 0.2.

#### 1.8 Kaolinite

Kaolinite is a naturally occurring mineral clay found mainly in the South of England and Central America. The clay samples used in the experiments described here were supplied by English China Clays International, Cornwall. Various pre-dispersed size fractions are available from a broad fraction with 80% by weight less than 2 microns to relatively narrow size distributions nominally from

0.4-(0.1)-1 microns. They are used for high quality paper coatings because of their scattering efficiency in the visible spectrum and nominally broader fractions are used as fillers 1-(1)-6 microns. The width of the size distribution within a fraction can be seen from the electron micrograph <sup>data</sup> shown in figures 1.4 and 1.5. Kaolinite is an aluminosilicate clay which possesses a two-layered crystalline structure with a unit cell shown schematically in figure(29) 1.6. The unit layer consists of a tetrahedral sheet of oxygen and silicon atoms linked by co-valent bonds to an octahedral sheet of hydroxyl groups, oxygen and aluminium atoms; the two sheets share common oxygen atoms. The basal spacing in kaolinite is 0.72nm between corresponding sheets in stacked unit layers. These layers are held together by weak van der Waals forces allowing cleavage to occur along parallel planes, producing the flat platelet structure observed in electron micrographs. Kaolinite particles are approximately hexagonal platelets with face diameters in the range 0.1 to 10 microns and a density of 2600 kgm<sup>-3</sup>. They can be approximated to thin discs with an aspect ratio of about 10:1[30]. It has been established[29] that the charge on the particle face is always negative due to isomorphic substitution of positive elements by elements of lower valency. At the edges the parallel arrays of tetrahedral silica sheets and the octahedral alumina sheets are disrupted and primary bonds are broken. The exposed surface is similar to the oxide surfaces of silica and alumina and hence the charge-determining mechanism of the

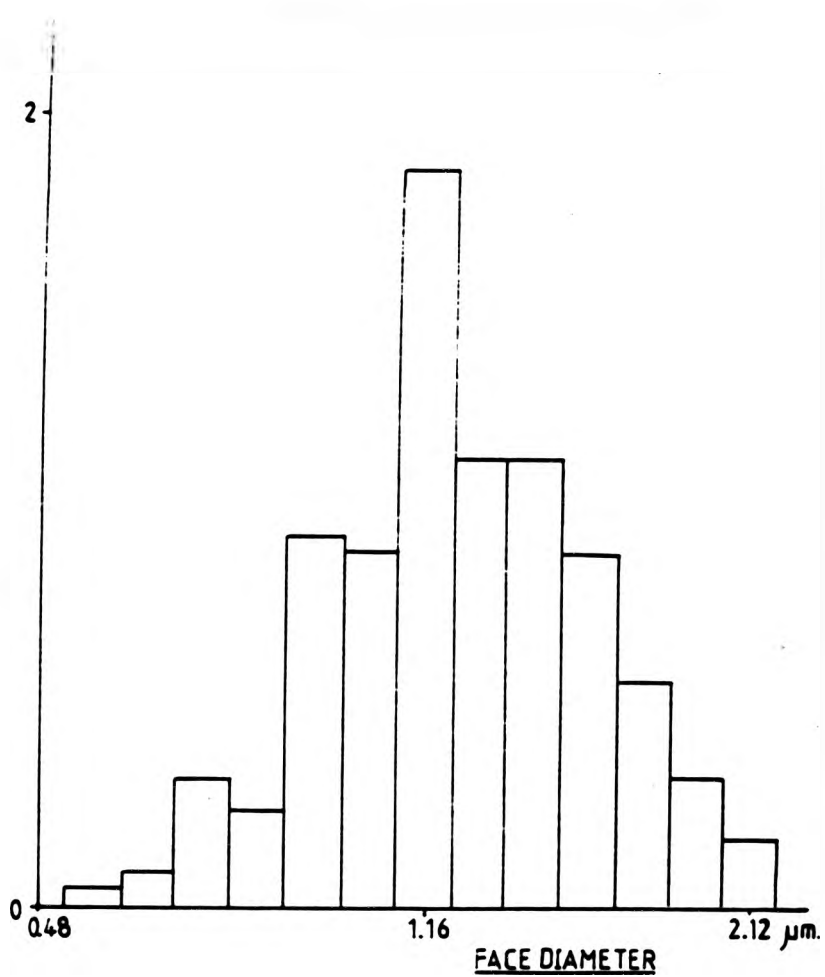


Figure 1.4 Distribution in particle face diameters obtained from scanning electron micrographs of a nominal 0.4-0.5 micron size fraction of kaolinite

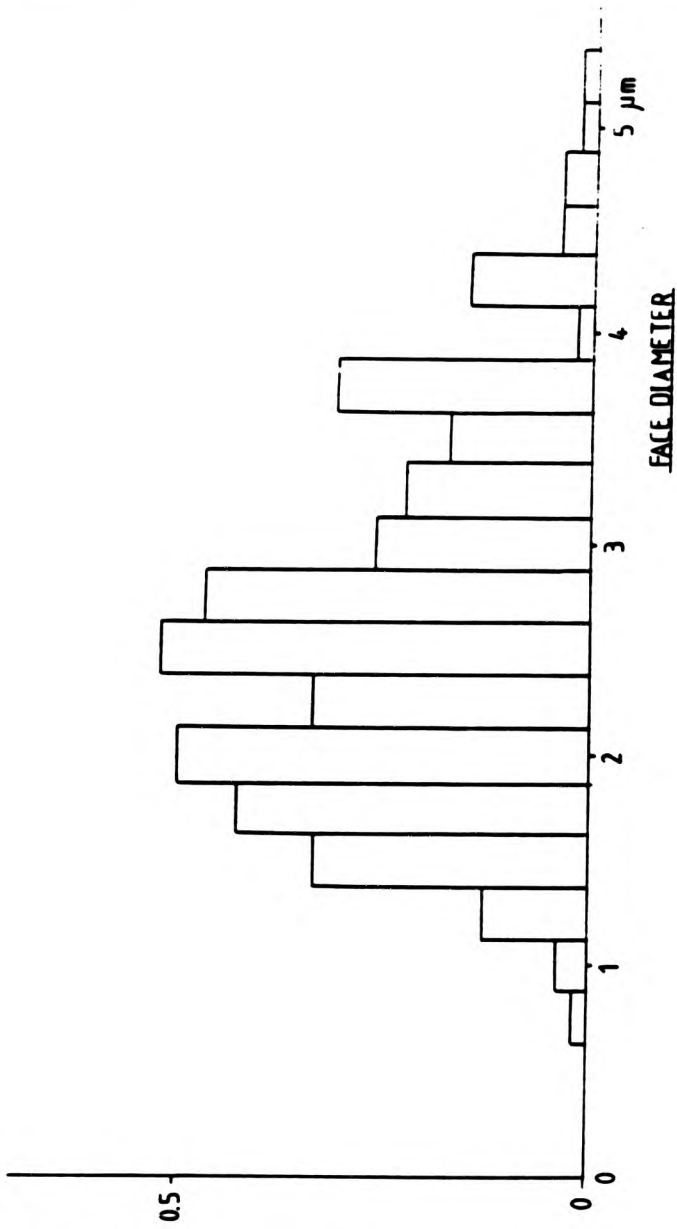


Figure 1.5 Distribution in particle face diameter obtained from scanning electron micrographs of a nominal 1-2 micron size fraction of kaolinite

edge is that of an oxide surface. Thus in the case of an hydrated oxide the neutral surface can be represented schematically as in figure 1.7a. This can ionise to give a negatively charged surface (1.7b) or adsorb a proton to give a positively charged surface (1.7c). The double layer at the edges is therefore formed by the adsorption of potential determining hydrogen and hydroxyl ions; thus the edge is positively charged below pH7 and negatively charged above pH7. The mode of aggregation is therefore dependent on the pH of the dispersion. At low pH the particles can flocculate in the face to edge mode due to the interaction of oppositely charged double layers; this gives rise to a "house of cards" floc formation[31]. At high pH a similar "house of cards" structure is formed as result of the interaction of the extended double layers[32] particularly at low electrolyte concentrations e.g. in water. This model accounts for the change in rheology with pH found in clay dispersions e.g. Tadros[33] found a minimum in the plastic viscosity at pH 7 for Bentonite dispersions. Similar results are available for kaolinite and are discussed below.

The stability of kaolinite dispersions is increased by the use of short chain polymer surfactants. In this work a polyacrylate neutralised with sodium was used, referred to by its trade name Dispex. Dispex is a polymer liquid containing 40% by weight sodium polyacrylate of molecular weight approximately 2000. In aqueous dispersions the acrylate groups ionise to give negatively charged COO groups on a carbon backbone. At low pH these groups can

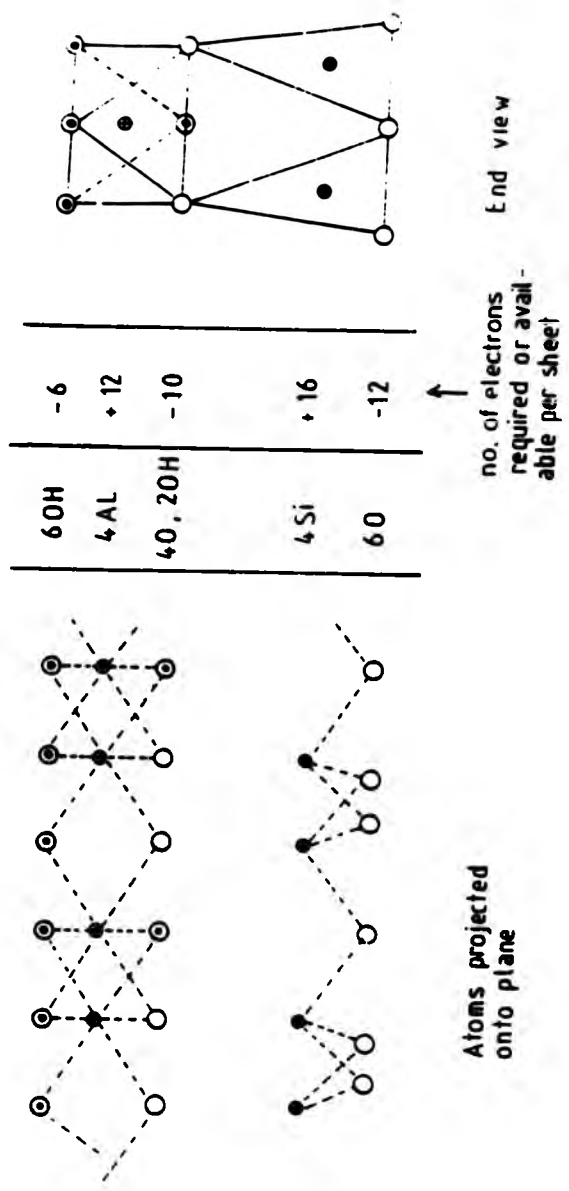
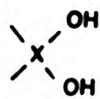
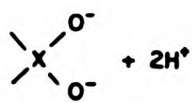


Figure 1.6 Schematic representation of the crystal structure of kaolinite

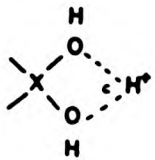




a)




b)



c)

Figure 1.7 Mechanism for *pH dependant* potential at the edges of kaolinite platelets

attach themselves to the positive particle edge, however it is reported[34] that greater stability is achieved when the polymer is added at pH8, also electron micrographs[34] show the polymer to be adsorbed at the particle edges. There seems to be no reference in the literature to account for this anomaly, however irrespective of the adsorption mechanism Dispex is used extensively in the paper-coating industry and provides the required dispersion stability. Measurements of dispersion viscosity against Dispex concentration[34] for kaolinite dispersions show a minimum viscosity which defines the optimum Dispex dosage for dispersion stability. The subsequent increase in viscosity on increasing the Dispex concentration is interpreted as evidence for re-flocculation. Two mechanisms have been put forward to explain this re-flocculation: Sommerauer[35] reported flocculation of negatively charged particles by negatively charged sodium polyacrylate in the presence of Calcium (20ppm). They suggested Calcium bridging between successive negative polymer sites as the agent responsible, i.e. doubly ionised Ca ions are adsorbed to separate polymer chains which are attached to separate particles, however the addition of excess Dispex may be the same as adding excess salt and therefore increasing the electrolyte concentration and introducing electrostatic instability. Measurements of the real refractive index of kaolinite particles by differential refractometry gave a value of 1.57[36]. The imaginary coefficient of refractive index is very low. This was checked[37] using an index matching



solution. It was observed that dispersions were transparent up to 50% solids.

#### 1.9 Dispersion preparation

In all the experiments conducted throughout this thesis the samples were prepared using the method described below.

Using a small glass pestle and mortar the samples of clay were mixed with deionised water, and Dispex when required, into a slurry with enough force to break up any aggregates.

This smooth paste was then diluted to the required concentration with a precisely measured amount of water.

The mixed sample was put into a sample bottle which was then sealed. When enough samples had been prepared in this way, each sample was sonicated in a Soniprep 150(MSE) at a probe amplitude setting of 14 microns to thoroughly mix the samples. After mixing, the sample pH was measured with a Philip Harris digital pH meter and adjusted by the addition of NaOH to increase the pH or  $\text{H}_2\text{SO}_4$  to reduce it.

After the pH had been adjusted in this way the samples were left to stand on the bench for 1 hour after which time the pH was then measured and re-adjusted if necessary. The samples were then sonicated and used immediately.

The period and amplitude of the sonicator were chosen after experimentation to reduce variations in the samples produced by errors in mixing times and amplitude.

## CHAPTER 2

### Measurement of the scattering parameter S in concentrated Kaolinite dispersions.

#### 2.1 Introduction

During the course of this work two main experimental techniques were developed in order to characterise the scattering properties of concentrated Kaolinite dispersions.

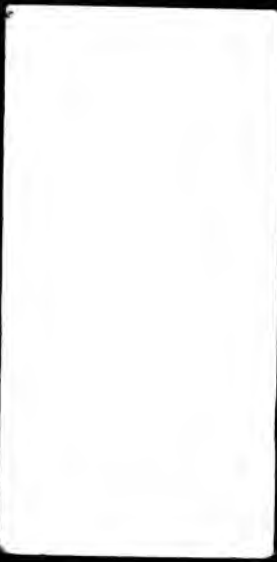
Initially transmittance measurements were made using a technique usually associated with single scattering measurements. This system was adapted to carry out measurements of the intensity transmitted through multiple scattering dispersions.

The transmittance technique proved to have limited applicability, giving useful results over the volume fraction range up to 0.05.

For measurements at higher concentrations this technique was abandoned in favour of a fibre optic diffuse reflectance system. This new system was designed to overcome the problems encountered using the transmittance system. The results obtained and the comparisons between these two techniques are presented below in chronological order.

#### 2.1.1 Transmittance measurements

A parallel collimated beam with a 20mm diameter was obtained using a tungsten source powered by a stabilised power supply and a simple lens system. This white source could be used with interference filters to produce



quasi-monochromatic light, but with a significant reduction of optical power. The collimated beam was incident on a variable path length cell (VPC) (Specac 8100) which could be adjusted to give path lengths in the range 0 to 10mm. The cell windows had a diameter of 25mm, and were removable for cleaning purposes. Also the body of the cell could be disassembled to facilitate cleaning.

The detection system consisted of an incoherent optic fibre cable of diameter 3mm which was fixed in place such that one end was in contact with the VPC exit window, the other end of the fibre illuminating a silicon photodetector. The D.C. output of this detector was amplified and displayed by a Macam 3000 photometer. Tests carried out using neutral density filters showed that the photometer reading was linearly related to the optical flux on the photodetector to within better than 0.1%. The apparatus is shown schematically in figure 2.1.

#### 2.1.2 Experimental procedure

The samples were prepared as described in chapter 1. The volume fractions used were from 0.01 to 0.05 Kaolinite in deionised water with 3% Dispex by weight of clay when required. In each case the pH was adjusted to the required value using the method described in chapter 1.

Before beginning each experimental run the VPC was cleaned with a detergent solution RBS 25 and then rinsed, firstly with distilled water and finally with acetone. The cell was then dried in a hot oven. After cleaning the VPC was fixed in its cradle with the path length set at 10mm. The

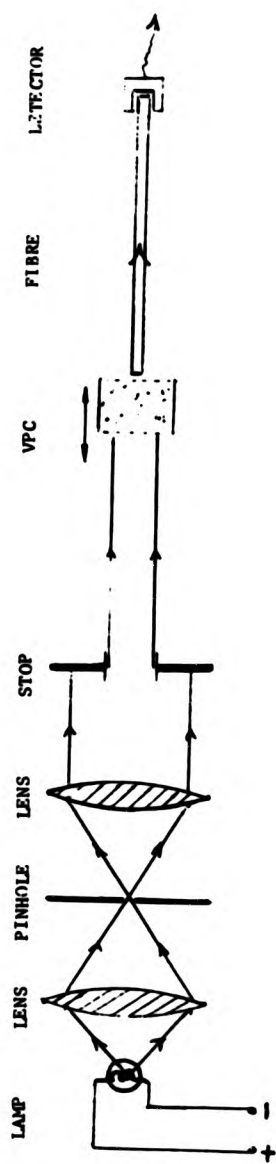


Figure 2.1 Transmittance apparatus employing the variable path-length cell (VPC)

prepared sample was then placed in the cell. Readings of the transmitted flux were then taken, starting at the high end of the path length range to ensure that no air bubbles entered the sample during the measurement cycle. The flux  $I_e$  was measured with a sample of deionised water. Experiments were carried out to investigate the variation of  $S$  with the equivalent stokes diameter (ESD); the variation of  $S$  with concentration; and the variation of  $S$  with pH.

#### 2.1.3 Variation of $S$ with ESD

To characterise the change in the scattering parameter  $S$  with particle size in the multiple scattering region of concentration, data were obtained from the VPC using the fractionated samples at a volume fraction of 0.01 in deionised water and 3% Dispex by weight of clay. In each case the sample pH was adjusted to 8.

Using a non-linear least squares algorithm the data were fitted to the Kubelka-Munk equation assuming zero absorption, as discussed in the previous chapter, i.e to a relation of the form

$$T = \frac{A}{1 + Sz} \quad (2.1)$$

where  $A$  is a constant required to account for the arbitrary units used in measuring the transmittance. An example of the fit obtained is shown in figure 2.2. It was found that the function used did not provide a very good fit especially at the intermediate points. However since this series of experiments were carried out at constant concentration it was felt that useful comparisons could

Transmittance (arbitrary units)

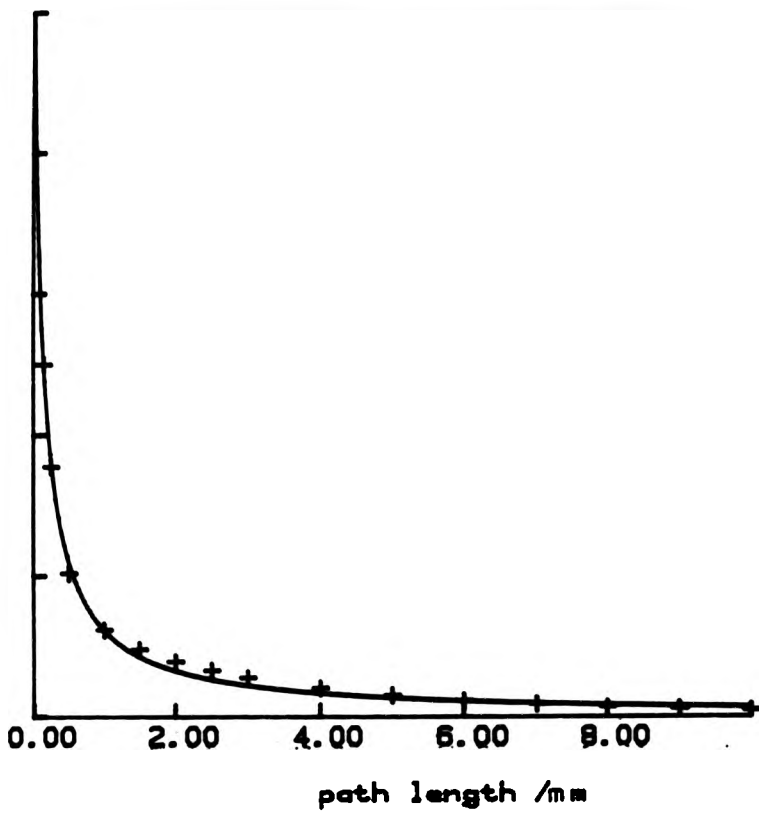


Figure 2.2 Example of data obtained using the (VPC) solid line - theoretical fit, points - experimental data



still be made.

The photon diffusion theory[8] predicts that for a system of spherical scatterers there will be a correlation between scattering angles reducing the measured  $S$  by the factor  $(1-\langle\cos\theta\rangle)$ , where  $\langle\cos\theta\rangle$  is the photon diffusion scattering angle function discussed in chapter 1, used to account for forward scattering in large particles. The magnitude of the term  $\langle\cos\theta\rangle$  is dependant on the single scattering properties of the dispersed phase such that for isotropic Rayleigh scatterers  $\langle\cos\theta\rangle = 0$  and for particles which scatter more light in the forward direction  $\langle\cos\theta\rangle > 0$ . Generally  $\langle\cos\theta\rangle$  increases with particle size. Wickramasinghe [38] has tabulated data obtained from the Mie theory for spheres and gives  $Q(1-\langle\cos\theta\rangle)$  where  $Q$  is the scattering efficiency and is proportional to the product  $SD$  where  $D$  is the particle diameter.

The results obtained showing the variation of  $S$  with ESD are shown in figure 2.3 together with a theoretical curve. It can be seen that the theoretical curve gives excellent agreement with data. However it should be noted that in order to fit the data the particle size diameter used for each volume fraction was  $ESD/2$  indicating an even distribution of faces and edges. In the absence of scattering theories for non-spherical particles it is difficult to make meaningful comparisons however the data clearly shows the optical resonance at about the  $0.7-0.8\mu m$  ESD size fraction observed in dilute single scattering dispersions and due to the similarity of particle size and mean wavelength.

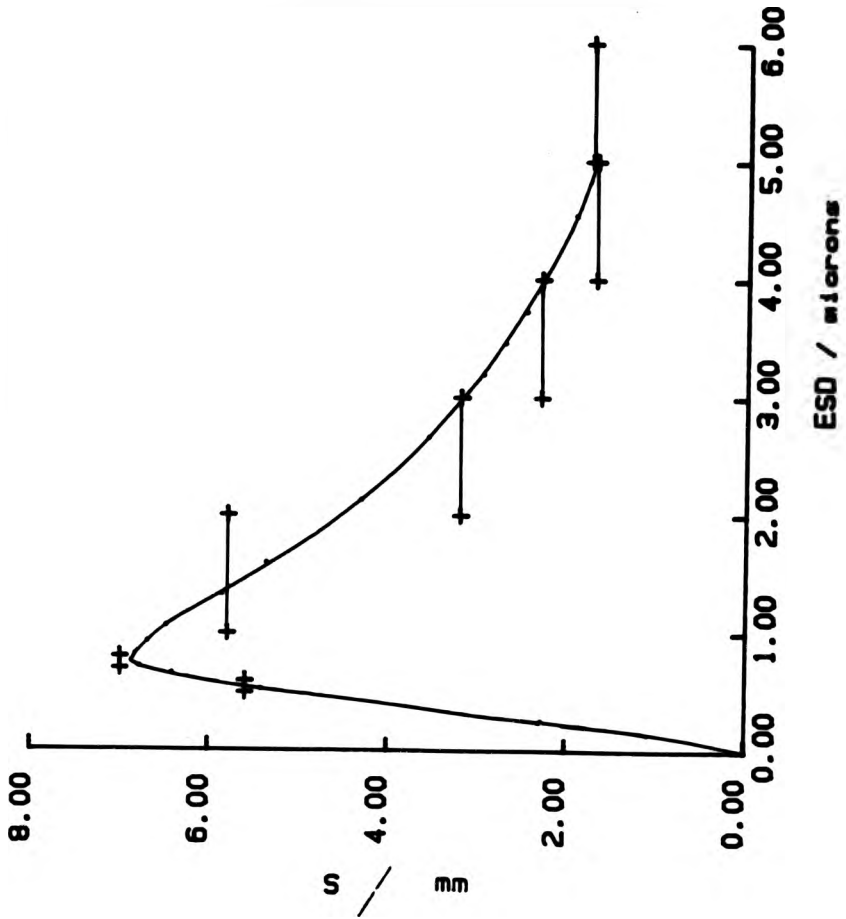


Figure 2.3 S as a function of ESD, for kaolinite samples at a volume fraction of 0.01, compared with theoretical data obtained using the Mie theory -solid line

#### 2.1.4 Variation of S with pH

In this series of experiments with sample volume fractions of 0.01 and 0.02 and 0.05 clay in deionised water, and no Dispex, S was measured for the 0.7-0.8, 1-2 and 3-4 micron fractions, at pH's in the range 4 to 9. For a pH of less than 4 the clay settled out in about one minute, and measurements could not be taken.

It is known that the pH of colloidal dispersions greatly affects the flocculation process e.g.[39]. However over the pH range used here there was no significant variation in the value of S measured. It was therefore concluded that although the samples were flocculated to varying degrees this did not produce a variation in the scattering properties of a randomly organised dispersion, i.e. even when groups of particles have a local ordering, the total scattering remains constant. This indicates that there is little or no optical interference between the particles due to their proximity. This can be explained in terms of the coherence of the optical probe. If the particles are at a separation greater than the temporal coherence length and the spatial coherence area of the light source even when flocculated, then there will be no optical interference effects. From optical theory [40] the temporal coherence length is approximately  $\lambda^2/\Delta\lambda$  where  $\lambda$  is the mean wavelength of light in the medium and  $\Delta\lambda$  is the width of the wavelength distribution. For white light this coherence length is thus of the order of  $\lambda$  or ~0.6 micron. Therefore particle centres that are separated by a distance

greater than this will not optically interfere. Also the van Cittert Zernicke(40) theorem defines a spatial coherence area as the area over which a partially coherent source will be coherent. The theorem gives this area as  $0.16\lambda a$  where  $a$  is the angular radius of the source. For diffuse light incident at a plane  $a = \pi$ , therefore for two particles situated in this plane to produce optical interference the interparticle separation must be  $< 0.03$  microns. The combination of these two effects seems to limit the usefulness of any techniques that rely on optical interference effects to the use of quasi-monochromatic light in a single scattering system for particles with dimensions greater than one wavelength.

#### 2.1.5 Variation of S with concentration

In this series of experiments samples of a broad clay fraction, with  $80wt\% < 2$ microns ESD, were prepared at increasing concentrations. However above volume fractions greater than about 0.05 equation 2.1 gave an increasingly poor fit to the data. This was thought to be due to the cell dimensions and the presence of path length dependant internal and external reflectances at the air/glass glass/sample interfaces. These reflectances are determined by the refractive index of the dispersion and the angular distribution of the incident flux. With collimated incident flux there is a continual transfer of collimated to diffuse flux and the relative intensities of these two components are path length dependant, therefore the

angular flux distribution is also path length dependant. The corrections necessary for the interfacial reflectances, therefore cannot be treated as constant. Also in both the two and four flux theories quoted in chapter 1, it is assumed that the samples are infinite in lateral extent. The range of optical depths over which this assumption holds can be defined using the useful empirical rule  $r/z > 8z$  where  $r$  is the cell radius and  $z$  is the path length. This therefore places a limit on either the concentration or the path length range for a given experimental system. In order to overcome the problems discussed above a reflectance cell was constructed which minimised the effects of windows.

## 2.2 Reflectance measurements

The method described here is shown to be superior to the usual integrating sphere method which requires large corrections to be made to allow for specular reflections at the sample surface. In order to make these corrections, accurate knowledge of the refractive index of the sample is required which is itself difficult to determine for highly turbid heterogeneous samples.

### 2.2.1 Apparatus

The reflectance cell is shown schematically in figure 2.4. The incident flux enters the sample through one arm of a bifurcated glass fibre bundle (Ealing Optical), where the diameter of the common end (B) was 3mm. A simple screw and dial gauge arrangement allowed the sample thickness  $z$  to be

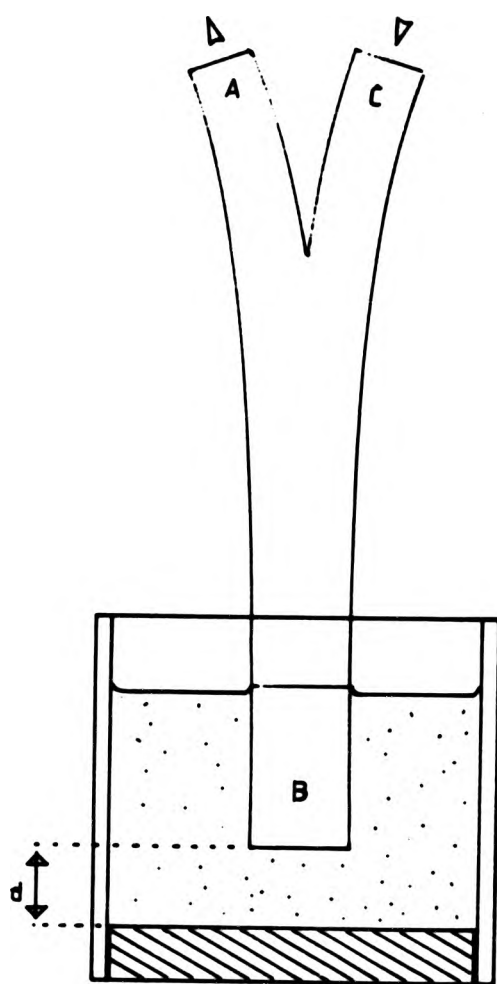


Figure 2.4 Schematic of the fibre optic reflectance cell

varied and measured. The sample cell was a black-bottomed cylindrical vessel of diameter 22mm. Diffuse flux reflected by the sample through the exit arm (A) of the bifurcated bundle illuminated a  $1\text{cm}^2$  silicon photodiode used in the photo-electric mode. The photocurrent was amplified and displayed by the Macam photometer used previously.

The diameter of each fibre was 125  $\mu\text{m}$  and the fibres from each arm were randomly mixed in the common bundle. The large number of fibres and the random position ensured that the illumination was uniform.

#### 2.2.2 Theory of the fibre bundle cell

This method was developed in order to minimise  $\rho$  and  $r'$  in equation (1.22).

Referring to figure 2.4 the influx suffers reflections at interfaces A and B, but since the optical influx and efflux routes were physically separate no externally reflected flux reached the photodiode, and  $\rho = 0$ .

Light scattered within the sample is internally reflected by the bundle in two ways:

- (i) at the common bundle-sample interface B; and
- (ii) after transmission through B at the arm-air interfaces at A and C.

The internal reflectance of the efflux by the whole of the bundle is easily shown to be

$$r' = r_0 + \frac{r_2 c^2}{1 - r_1 r_2} \quad (2.2)$$

where  $r_0$  is the internal reflectance of the flux from the sample by the common bundle-sample interface B. The second term describes multiple reflections of flux within the

glass fibres at the glass-sample interface B and glass-air interface at A and C,  $r_1$  and  $r_2$  are the reflectances for light within the fibre at B and A or C respectively, and  $\tau$  is the intrinsic transmittance of the fibre.  $c$  is the fraction of the total flux from the sample incident on the end of the bundle which is converted to propagating flux within the fibres of the bundle. Although there is a large refractive index mismatch between a glass fibre ( $n=1.56$ ) and air, its effect on  $r'$  is minimised by the small value of  $c$ , which is a function of the fractional area of the bundle taken up with glass core, the numerical aperture of the fibre and the refractive index of the glass relative to that of the sample. For the bundle used here  $c \sim 0.05$ ,  $r_1 \sim 0.01$  and  $r_2 \sim 0.05$ . Using the manufacturer's data  $\tau \sim 0.7$ , giving 0.001 for the term in  $c$ . The value of  $r_0$  estimated using Judd's method[9] applied to the three separate reflecting materials at the end of the common bundle, these were the core, cladding and epoxy resin with refractive indices 1.56, 1.46, 1.58 respectively (all at Na D line) and relative areas 0.14:0.76:0.10. Using these values and Judd's calculation of internal reflectance we have  $r_0 \sim 0.04$  for sample refractive indices in the 1.3-1.5 range occupied by most fluids, showing that  $r_0$  is the dominant term in equation (2.2) above. Putting  $\mu = 0$  and  $r' = 0.04$  in equation (1.22) shows the intrinsic reflectance is always within  $< 4\%$  of the measured value. This error was considered small enough to neglect in the subsequent analysis.



### 2.2.3 Initial experiments

The cell reflectance with a sample of deionised water ( $R_w$ ) was measured and compared with reflectance measurements ( $R$ ) from an S.P.S (broad size fraction 80 wt%  $< 2 \mu\text{m}$ ) sample at a volume fraction of 0.04. The ratio  $(R + R_w) / R$  was found to be a maximum of 1.02 at the lowest path length used of 0.15mm. This small error arising from the small but finite cell reflectance was deemed negligible in the light of the previous discussion on the limitations of the theory.

Using an SPS sample of volume fraction 0.2 reflectance measurements were made using two separate cells, one with white walls and one with black walls. The  $S$  values determined from these two data sets agreed within the experimental error and it was therefore concluded that the cell diameter was large enough to be considered semi-infinite in lateral extent.

### 2.2.4 Variation of $S$ with concentration

Samples were prepared in the volume fraction range 0.05 to 0.25, in each case the sample pH was adjusted to 8. This was done because although  $S$  is independent of pH in non-oriented samples, at pH8 Kaolin dispersions have a greater stability than at lower pH's due to double layer repulsion while having a low enough viscosity so that samples were easier to work with, thus reducing possible errors caused by e.g. trapped air bubbles.

The reflected intensity was measured over the path length range 0.15mm to 1.5mm for three samples at each

concentration. The data were fitted to the the Kubelka-Munk reflectance equation,

$$R = \frac{ASz}{(1 + Sz)}, \quad (2.3)$$

where the constant A is used to account for the arbitrary units used in measuring reflectance. A is the input intensity i.e.  $R = A$  when  $z$  is infinite. The fit using this function gave an error of about 4% and although this error is acceptable in the light of the previous discussion it was found that the value of  $S$  obtained from the fit varied markedly for small variations in the experimental data. Greater functional stability and a better fit were obtained by using the empirical function,

$$R = B(1 - \exp(-Sz)), \quad (2.4)$$

an example of the data obtained can be seen in figure 2.5 where comparison of the two fitting functions is made.

Figure 2.6 shows the variation of  $S$  with concentration where the  $S$  values plotted are those obtained using both the theoretical and empirical function. It can be seen that independent of the fitting function used  $S$  is a non-linear function of the concentration.

Fitzwater[41] has presented similar data for  $TiO_2$ . The decrease in  $S$  per particle with concentration is explained in terms of a dependant scattering theory for the sub micron pigment particles. In the experiments conducted here on large particles with incoherent illumination the conditions for dependant scattering are not fulfilled. However good agreement is obtained between theory and experiment by using the Mie theory with a concentration dependant relative refractive index, as used by Gate[42] to account for the decrease in scattering per particle with

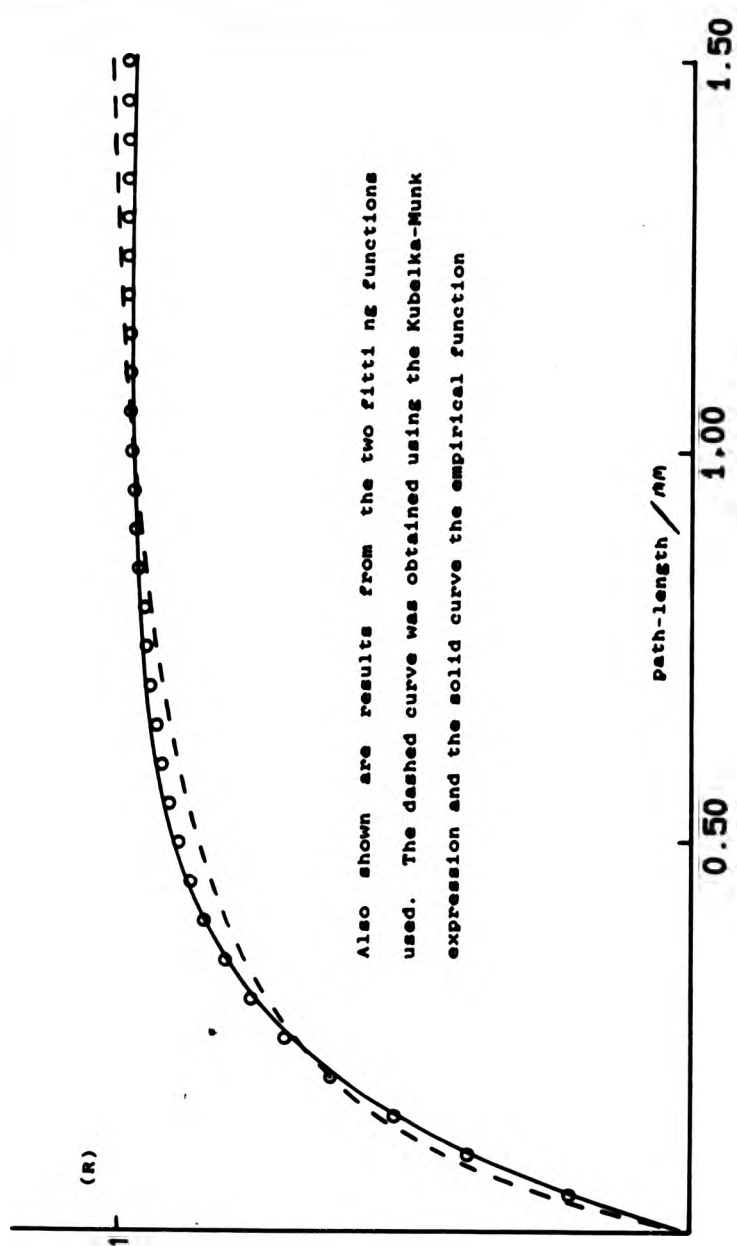


Figure 2.5 Example of data obtained using the reflectance cell. The kaolinite sample used was SPS at a volume fraction of 0.1

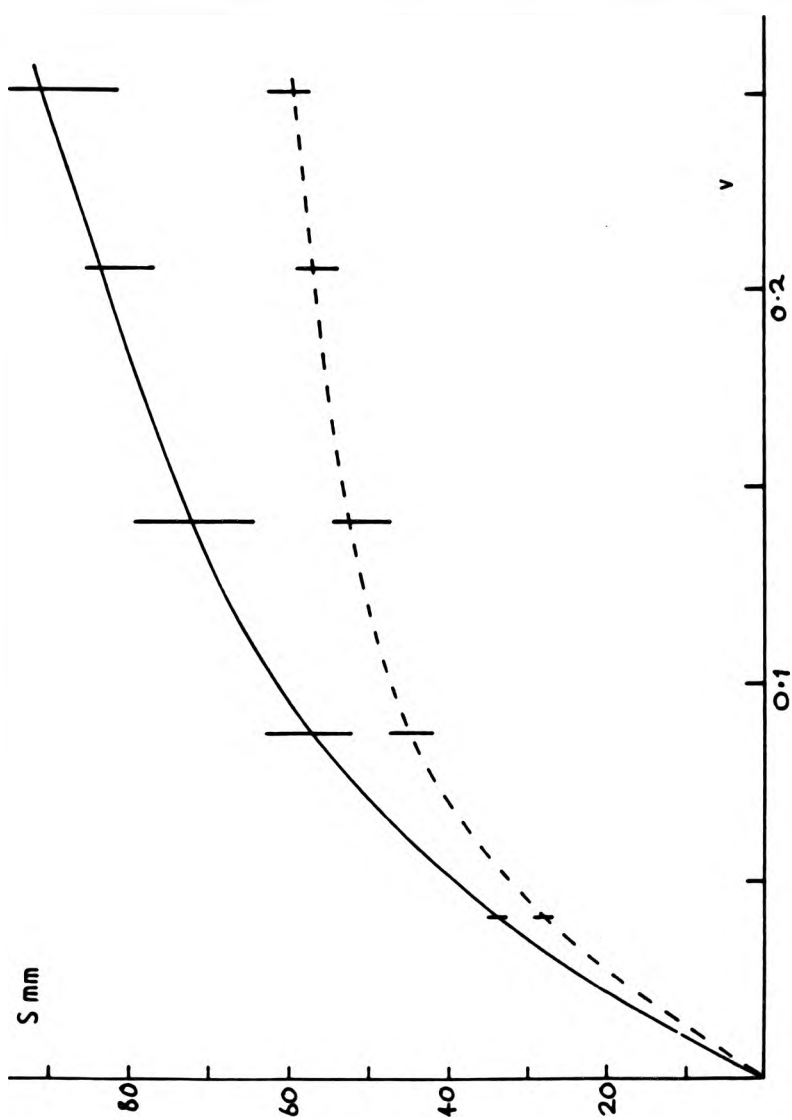


Figure 2.6  $S$  as a function of dispersion volume fraction  $v$  for samples of SPS. The solid line is calculated using the Kubelka-Munk equation 2.3 and the dotted line is calculated using equation 2.4

concentration for latex dispersions. Using a simple volume-weighted model, Gate[42] writes the relative refractive index as

$$n_r = \frac{n_p}{(n + v(n_p - n))}$$
. Where  $n_r$  is the relative refractive index,  $n_p$  is the particle refractive index,  $n$  is the refractive index of the suspending medium at infinite dilution and  $v$  is the volume fraction. In figure 2.7 the scattering efficiency per particle ( obtained by dividing  $S$  by the volume fraction ) is plotted against the volume fraction, the data are normalised to 1 for zero volume fraction. The theoretical curve obtained using the Mie theory is also plotted on the same graph.

Theory and experiment show excellent agreement although it should be noted that the system under investigation is a sample of polydisperse non-spherical particles, in contrast with the mono-disperse spheres assumed in the Mie theory.

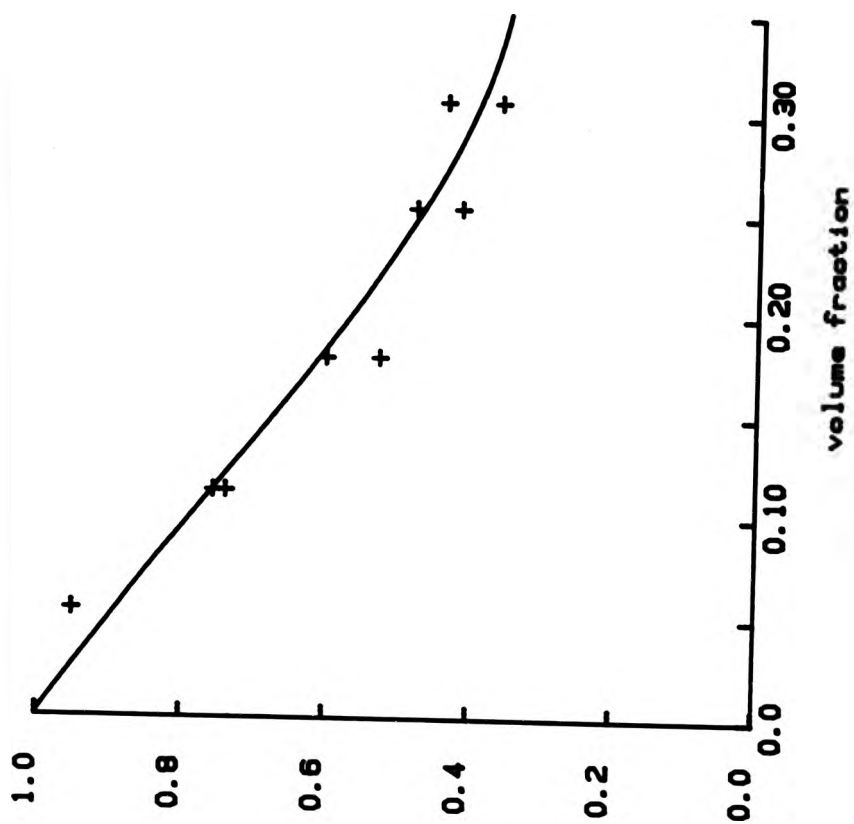


figure 2.7 Scattering per particle  $(\frac{s_v}{v})$  as a function of the volume fraction  $v$  for samples of SPS. The solid line, obtained from the Mie theory using a concentration weighted index of refraction, is compared with data obtained using the reflectance cell

## CHAPTER 3

### Experimental investigation of magnetic orientation.

#### 3.1 Introduction

It is well known[43] that the anisotropy of particles or flocs can be detected optically if the concentration is low enough for multiple scattering to be neglected. One such method[43] relies on the detection of the coherently transmitted light (i.e. the non-scattered intensity) transiting a dilute dispersion, by measuring the non-scattered transmittance with and without an aligning field. A measure of the particle or floc anisotropy is obtained since an oriented array of non-spherical particles will have a different geometric and scattering cross-section from a random array.

Measurements reported in this thesis were carried out on multiple scattering dispersions where each detected photon has undergone, on average, more than one scattering event. It might be assumed therefore that information on the orientation of particles within the dispersion will be averaged out and lost since the detected light flux is diffuse and spatially incoherent. This is shown not to be the case both empirically by the data obtained in this and subsequent chapters and theoretically by the following simple analysis. This analysis will show that a diffuse scattering cross-section is obtained when a sample is illuminated with isotropic flux and that the diffuse scattering cross-section is dependant on the orientation of

the scatterer. Having obtained this diffuse scattering cross-section it is then possible to infer the orientation of particles from the measured diffuse transmittance or reflectance given by the Kubelka-Munk type theories.

Thus information on particle or floc anisotropy is retained even when completely isotropic flux is used and this provides the theoretical basis to account for the data presented in this and the following chapters.

The following assumptions have been used in the analysis:

i) For optically dense media the angular dependence of the incident flux is quickly averaged out inside the sample due to multiple scattering, such that the radiance is taken as diffuse i.e. constant with angle.

ii) the dispersion is made up of sufficiently large particles such that their scattering cross-section is simply twice their geometric cross-section. This is the diffraction limit scattering cross-section.

iii) The particle model used is an oblate spheroid with symmetry <sup>semi-</sup>axis  $a$ , <sup>the other</sup> semi-axes  $b$  and axes ratio  $p = a/b$ .

In general for a flux direction normal to the  $(x,y)$  plane the radiance is defined as  $I(\theta, \phi)$  in figure 3.1. The particle orientation is defined by  $\Pi(\eta, \xi)$  where  $\Pi$  defines the particle normal.

The projection of the scattering cross-section of an oblate spheroid on the incident plane is then given by

$$C(\epsilon) = Q(\epsilon) \pi b^2 (\cos^2 \epsilon + p^2 \sin^2 \epsilon)^{\frac{1}{2}} \quad (3.1)$$

where  $Q(\epsilon)$  is the scattering efficiency of the particle and

$$\cos \epsilon = \cos \zeta \sin \eta \cos \phi \sin \theta + \sin \zeta \sin \eta \sin \phi \sin \theta + \cos \eta \cos \theta \quad (3.2)$$



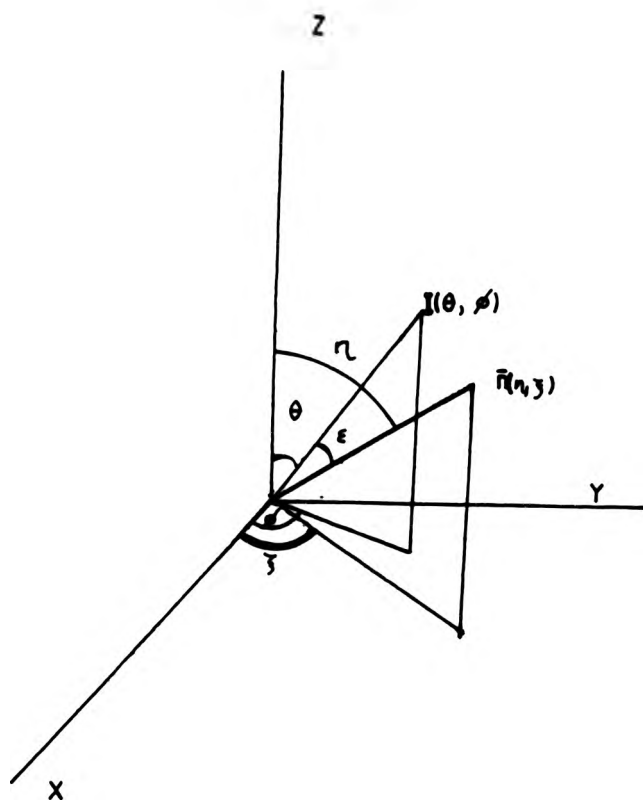


Figure 3.1 Coordinate system defining the particle orientation relative to the flux direction

The diffuse scattering cross-section  $C_d(\eta)$  is assumed to be given by  $C(\xi)$  weighted according to the radiant intensity  $I_e(\theta, \phi)$ . The diffuse scattering cross-section is given by

$$C_d(\eta) = 2\pi b^2 \frac{\int_0^{2\pi} \int_0^{\pi/2} C(\xi) I_e(\theta, \phi) \sin\theta \, d\theta \, d\phi}{\int_0^{2\pi} \int_0^{\pi/2} I_e(\theta, \phi) \sin\theta \, d\theta \, d\phi} \quad (3.3)$$

With the assumption of diffuse flux we can use the Lambert cosine law to find  $I_e(\theta, \phi)$  i.e.

$$I_e(\theta, \phi) = I(\theta, \phi) \cos\theta \quad (3.4)$$

since  $I$  is constant with angle we have

$$C_d(\eta) = 2\pi b^2 \int_0^{2\pi} \int_0^{\pi/2} C(\xi) \cos\theta \sin\theta \, d\theta \, d\phi \quad (3.5)$$

using the diffraction limit of the scattering cross-section,

$$Q(\xi) = 2$$

Even with these simplifications the integration cannot be solved analytically as it stands. An analytical solution is possible however if  $C(\xi)$  is expanded in a series of Legendre polynomials. Since  $C(\xi)$  is a function of  $(\cos \xi)$  we have

$$C(\xi) = 2\pi b^2 \sum_n a_n P_{2n}(\cos \xi) \quad (3.6)$$

This integration is easily solved using the recurrence relationship for the Legendre polynomials to give,

$$C_d(\eta) = 2\pi b^2 \sum_n a_n b(n) P_{2n}(\cos \eta) \quad (3.7)$$

where  $b(n)$  is defined by integration of the recurrence

relationship.

This gives for an axis ratio  $p = 0.1$  (3.8)

$$C_d(\eta) = (0.489 + 0.279 \cos^2 \eta - 0.047 \cos^4 \eta + 0.0157 \cos^6 \eta + \dots) \times 2\pi b^2$$

For the three cases of most interest namely face on; edge on and random orientation, the diffuse scattering cross-section is given by,

$$C_d(0) = 2\pi b^2 (0.724) \quad (3.9)$$

$$C_d(90) = 2\pi b^2 (0.489) \quad (3.10)$$

$$C_d(\text{RANDOM}) = 2\pi b^2 (0.57) \quad (3.11)$$

The single scattering results for  $p = 0.1$  give,

$$c(0) = 2\pi b^2 \quad (3.12)$$

$$c(90) = 2\pi b^2 (0.1) \quad (3.13)$$

$$c(\text{RANDOM}) = 2\pi b^2 (0.55) \quad (3.14)$$

These results show quite clearly that although some information is averaged out there is still information on particle shape to be obtained from the diffuse light scattered by optically dense media. It is therefore possible to use multiple scattered light as a probe of particle orientation in an applied field. It should be noted that the value obtained for random orientation in the two cases should agree, this therefore defines an error of about 4% caused by truncating the series in equation 3.8 after four terms. The values should agree since under random conditions the scattering is independent of the angle of incidence. In a single scattering experiment only one angle is used and for multiple scattering all angles are used.

ESD Fraction (μm)	Fe <sub>2</sub> O <sub>3</sub> %	Iron as Fe	Mica %
0.4 - 0.5	0.37	0.259	2.6
0.5 - 0.6	0.37	0.259	2.9
0.6 - 0.7	0.39	0.273	3.7
0.7 - 0.8	0.41	0.287	4.9
0.8 - 0.9	0.46	0.322	6.5
1.0 - 2.0	0.44	0.308	8.0
2.0 - 3.0	0.55	0.385	13.5

Table 3.1 chemical assay of kaolinite fractions

Since kaolinite contains magnetically active impurities (see the discussion in chapter 1) it is possible to induce orientation by the application of a magnetic field. A chemical assay showing the impurities of some of the fractionated clay samples used in this work is shown in table 3.1. In view of the existence of these impurities it was decided to study the effect of magnetically induced orientation on the optical transmittance of kaolinite samples i.e. to measure the difference between the scattering cross-sections of random and oriented non-spherical particles. There are two approaches possible: a) to apply an alternating field and measure the frequency response of the samples and the phase difference between the optical response and the applied field; and b) to apply a d.c. field and measure the amplitude and relaxation process.

To carry out measurements in the frequency domain a 200 watt a.c. amplifier was constructed to power a Helmholtz pair. This gave a maximum field strength of the order of 0.1T in the frequency range 0 to 500Hz. It was initially decided to take measurements on sample dilutions where single scattering was dominant. However due to the problems discussed in the introduction the signal was lost in the noise and although a phase sensitive detector was used in an attempt to recover the signal, useful results were not obtained.

Using a fast Fourier transform and the analogue-to-digital converter of a BBC microcomputer the frequency spectrum of the random variation of intensity with time, in the absence

of an applied field, was obtained. This showed the noise to be in the range 0-Hz. This means that for reproducible, useful (i.e. resolvable) results the statistical properties of the sample should not change over the total sampling period. Thus for a 255 point transform times greater than  $255/f$  are required to resolve a signal of frequency  $f$  i.e. several hundreds of seconds. Since the density mismatch between water and kaolinite is large, settling changes the statistical properties over this time, hence limiting the usefulness of data acquired in the frequency domain.

Other attempts were made to characterise the noise but with little success. It was finally decided that further attempts should not be pursued at this stage.

The problems so far encountered have been discussed in the introduction. In order to overcome them the sample concentration was increased such that multiple scattering became dominant.

### 3.2 Apparatus

The apparatus used in this series of experiments is shown schematically in figure 3.2. It consists of an optical input system, an electromagnet with hollow pole pieces and an optical detection system.

The optical components used are those already described in chapter 2 and used throughout this work. In these experiments however, the collimated beam diameter was reduced to 5mm to allow the beam to be transmitted through the pole pieces of the Leybold magnet.

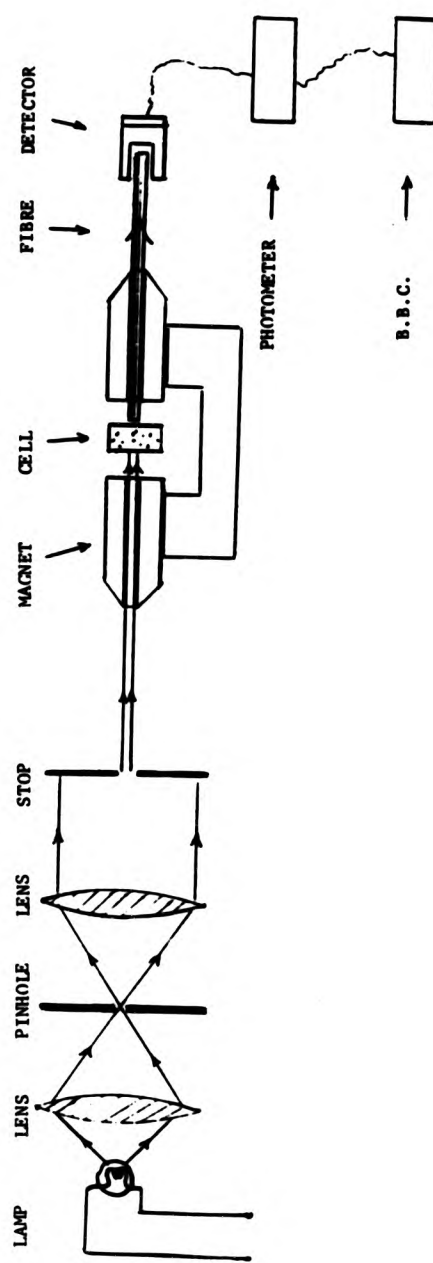


Figure 3.2 Schematic diagram of the apparatus used in the experiments on magnetic orientation

The magnet used had a coil resistance of 0.6 ohms at 5A. and was powered by a Farnell stabilised power supply. With a pole separation of 10mm a maximum field strength of 0.3T was obtained. To achieve this field strength an induction current of 8A was required. This necessitated the use of a small electric fan to cool the magnet coils and thus keep the field strength constant over time periods varying from 10s upto 8 minutes. Figure 3.3 shows the variation of field strength with induction current for a 10mm pole separation. The pole separation of 10mm was chosen to give a constant field strength across the sample and to allow ease of access ensuring accurate cell positioning.

For complete orientation field strengths of the order of Teslas(10) are necessary, however, useful results are still obtained when only partial orientation is achieved. In figure 3.4 the magnetically induced fractional change in turbidity is plotted as a function of field strength for a typical sample, this illustrates that complete orientation is not achieved with the field strengths available from the magnet used. A 2mm path length cell was used to contain the sample, the path length being chosen to ensure that multiple scattering was dominant over the concentration range used.

The field strength was monitored by a Hirst FM75 Gaussmeter, the analogue output from the Gaussmeter provided a trigger for a BBC microcomputer. Outputs from the Gaussmeter and the detection system were monitored by the microcomputer using two channels of its four channel analogue to digital converter. A programme was written



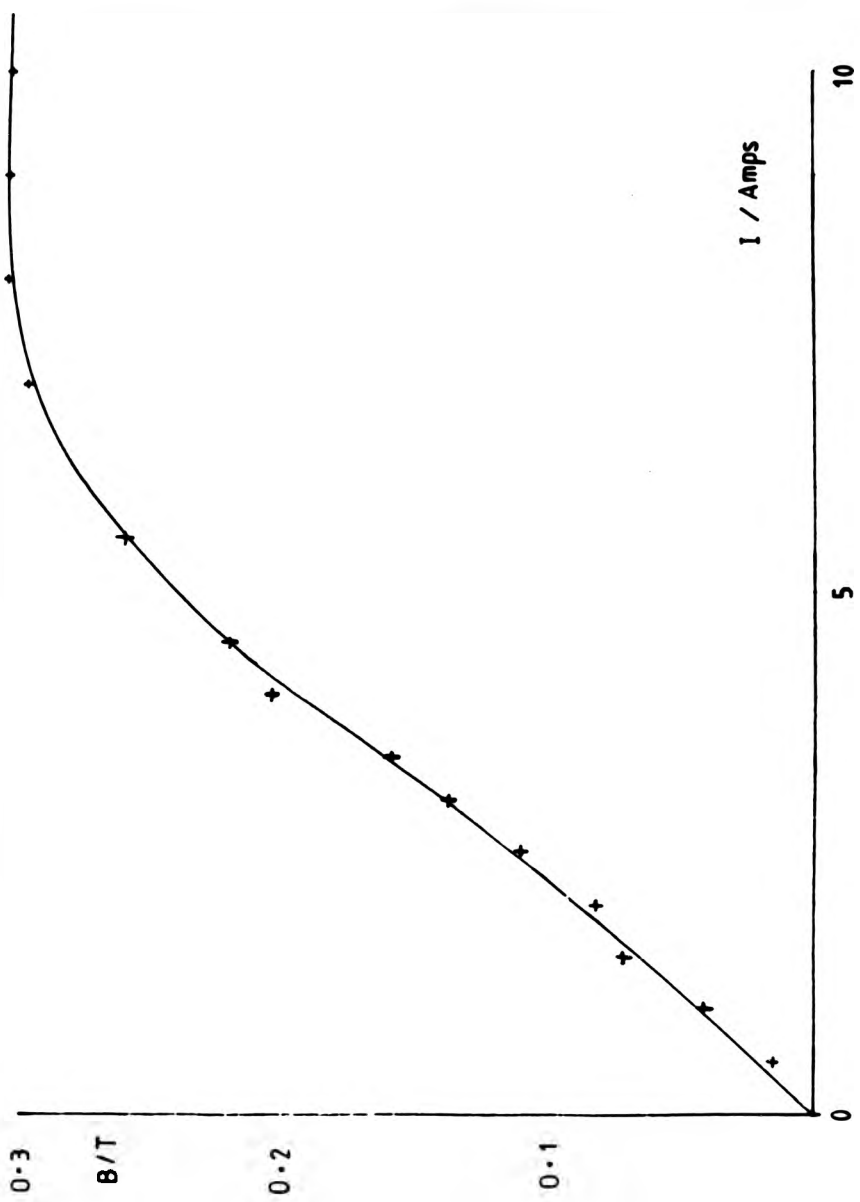


Figure 3.3 Field strength  $B$  as a function of coil current in the Laybold electromagnet

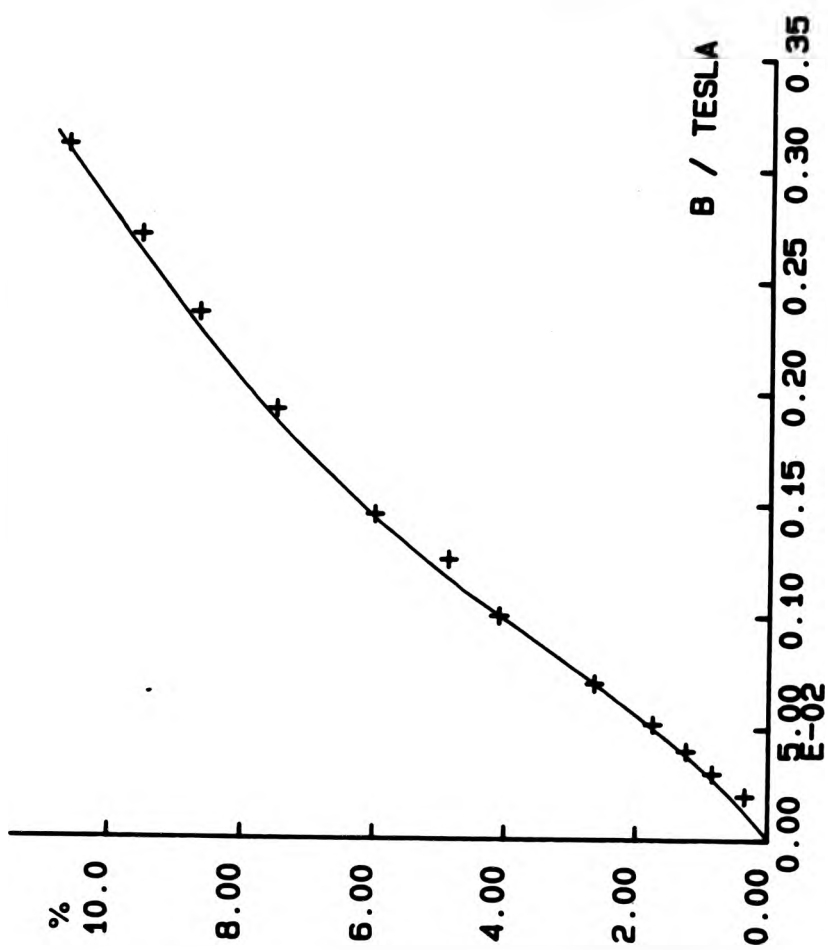


Figure 3.4 The percentage change in transmittance as function of field strength for a typical sample (SPS at a volume fraction of 0.05)

which initiated data collection the instant the field was turned off.

The cell was thoroughly cleaned before each experiment by placing it in a sonic bath filled with RBS25 cleaning solution. This was done in order to remove any sample deposits from the cell walls.

### 3.3 Initial experiments

The response time of the system was checked using Baal clay which has a high ferric impurity and it is therefore very easy to achieve full orientation with the magnetic fields available and in the absence of the field this orientation decays very rapidly. The time constant (the time for the detected optical signal to fall to  $1/e$  of its initial field on value) measured here was  $< 0.1$  s. i.e. about 10 times smaller than the time constants measured for kaolinite. The response time of the system was therefore taken as  $< 0.1$  s. The amplitude resolution of the system was  $< 0.1\%$ . This was measured by using non-magnetic but turbid suspensions of polystyrene spheres and measuring the spurious transmittance change with and in the absence of the field.

### 3.4 Experimental procedure

To ensure reproducibility of results all of the samples used in each experimental run were prepared on the same day and shaken by a mechanical shaker for thirty minutes before each experiment. The cell was then filled from a pipette and positioned between the poles of the magnet. The fibre

optic detection cable was then pushed up to the cell retaining the cell in position. The field was then applied until the photometer gave a steady reading. The computer programme was then initiated, which monitored the field strength and the photometer output. The field was then removed and the computer began its recording cycle.

The total data acquisition time and the time interval between each data point was varied, to take into account the variation in relaxation times.

The samples were prepared using the method described in chapter 1 and experiments were carried out in order to investigate the following: the concentration; pH; surfactant concentration and particle size dependence of the magnetically induced turbidity change.

#### 3.5 Variation of the transmittance change with concentration

Measurements were carried out using a broad particle size fraction ( $> 80\text{wt}\%$  below 2 microns) with a pH adjusted to 8. The volume fraction of clay in de-ionised water was varied between 0.02 and 0.2. The results are shown in figures 3.5 and 3.6.

In figure 3.6 relaxation time is plotted against concentration. The data obtained from this series of experiments, an example of which is shown in figure 3.7, cannot be characterised by one exponential function. It was therefore decided to define the time constant as the time taken for the amplitude to fall to  $1/e$  of its initial value. This was done since multi-exponential data fitting

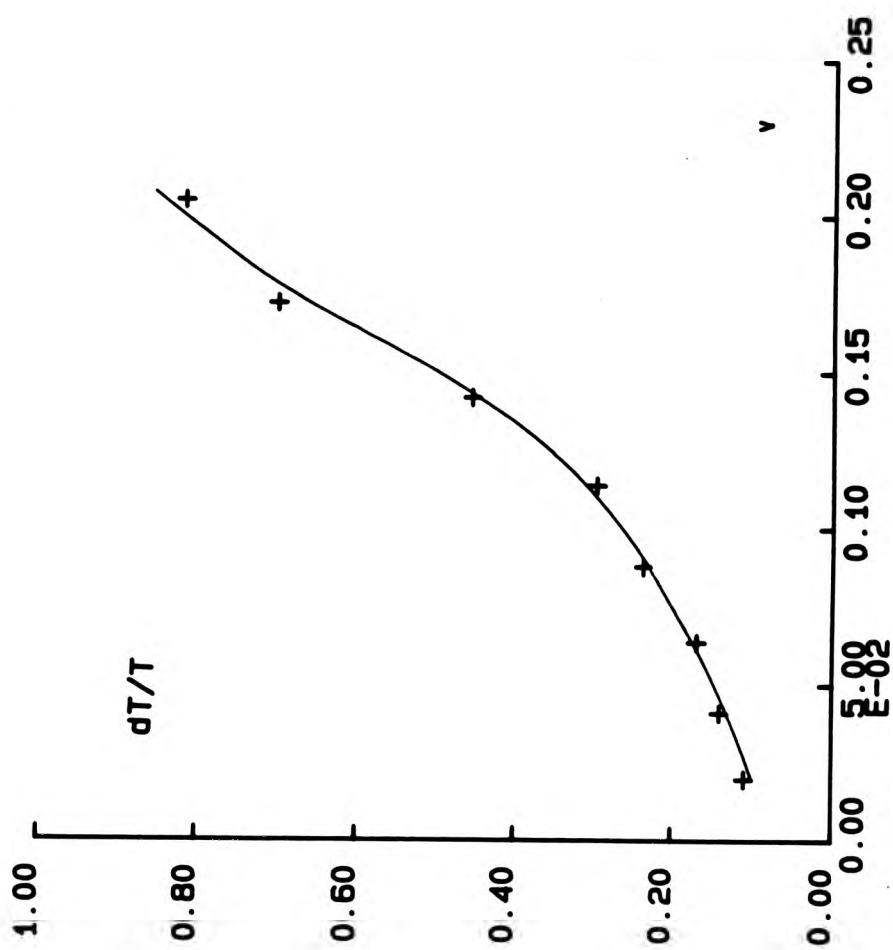


Figure 3.5 The relative change in  $T$  as a function of volume fraction  $v$  for SPS dispersions

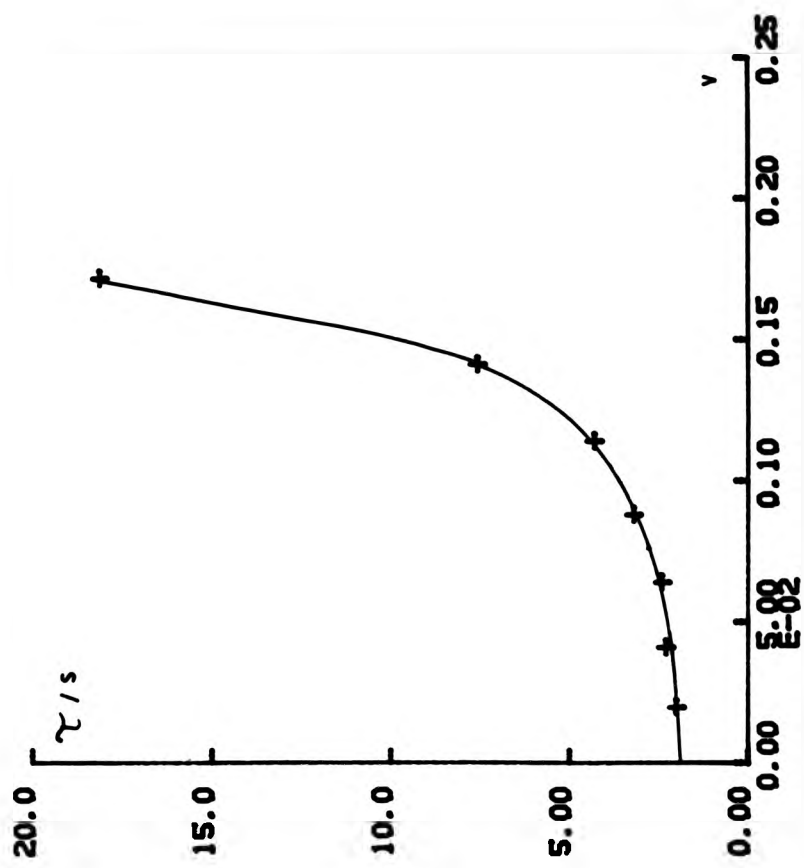


Figure 3.6 Relaxation time as a function of volume fraction for SPS dispersions

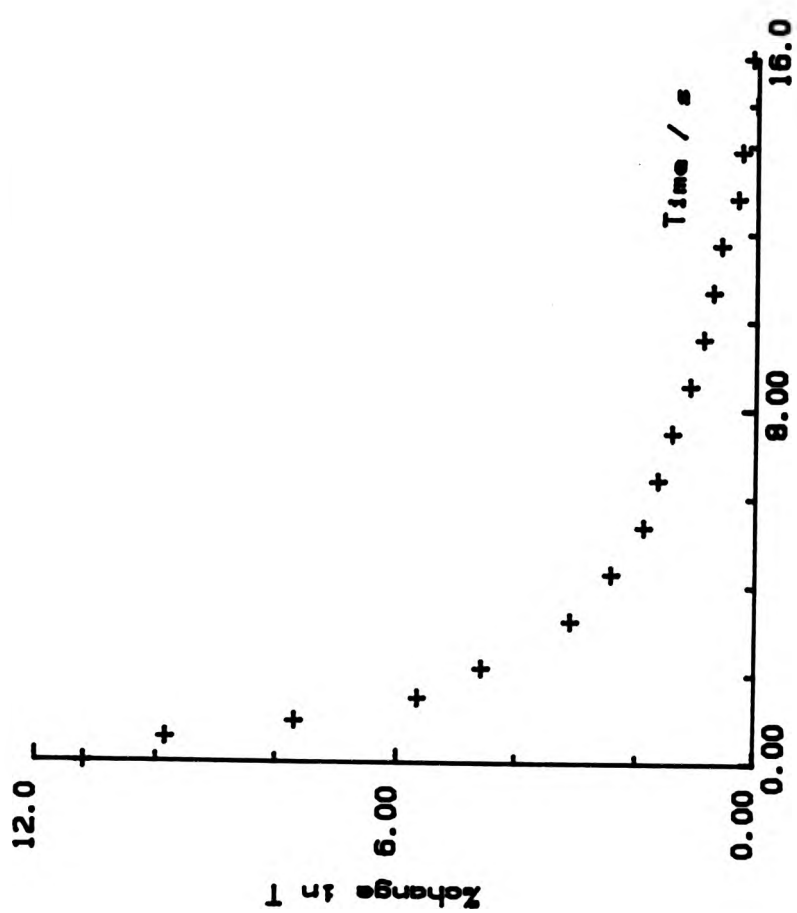


Figure 3.7 An example of the data obtained in the opto-magnetic experiments. A sample of the 0.7-0.8 micron kaolinite size fraction at a volume concentration of 0.05

algorithms were found to be inaccurate. Differentiating the Kubelka-Munk expression for Transmittance with respect to S gives the fractional change in T to be

$$dT/T = -dS/S Sd/(1+Sd). \quad (3.15)$$

For a constant fractional change in S and a constant path length the fractional change in T with concentration should increase asymptotically to the value  $dS/S$ . Since the data does not behave in this way we must conclude that the fractional change in S is not constant with concentration but increases with increasing concentration.

The disorienting influence of Brownian motion is likely to decrease with concentration and this is evidenced by the increase in the relaxation time with concentration. However in order to test this hypotheses we require a strong enough field to achieve total orientation at all concentrations, it would then be possible to measure the field strength required to give total orientation as a function of the concentration, in the present experimental system this is not possible to achieve with kaolinite.

### 3.6 Variation of the transmittance change with pH

It is well documented that the stability of kaolinite dispersions is strongly pH dependant, e.g. see the discussion in chapter 1.

Here the fractional change in transmittance induced by applying an external D.C. magnetic field is used as an indicator of the ability of the particles or flocs to orient in the applied field and therefore as a monitor of the state of flocculation or deflocculation of a



concentrated dispersion.

It has been already shown in chapter two that there is no flocculation induced change in the scattering parameter  $S$  of undisturbed dispersions as measured in a multiple scattering regime using a white light source. Here however the fractional change in  $S$  is investigated via the fractional change in transmittance. It has been shown above ( section 3.1 ) that orientational information is retained in optically dense multiple scattering systems. The fractional change in transmittance is thus a measure of the eccentricity of the particles or flocs which make up the dispersion under investigation.

For dilute kaolinite dispersions Tadros<sup>(38)</sup> has shown that the point of zero charge for the edge of clay platelets lies between pH6 and pH7. Below this pH the particles flocculate in a face to edge mode so that for a large enough floc there will be no change in transmittance since the floc will be orientationally isotropic. As the floc size decreases the transmittance change will increase to a maximum for single particles since single particles will have the largest anisotropy of magnetic moment and axis ratio. Therefore using this technique it is possible to monitor the flocculation process in Kaolinite or any other system of magnetically anisotropic non-spherical particles.

The volume fractions used were 0.01, 0.02 and 0.07 kaolinite in de-ionised water, with no Dispex added. The sample pH was adjusted using sodium hydroxide and sulphuric acid solution. The results are shown in figure 3.8.

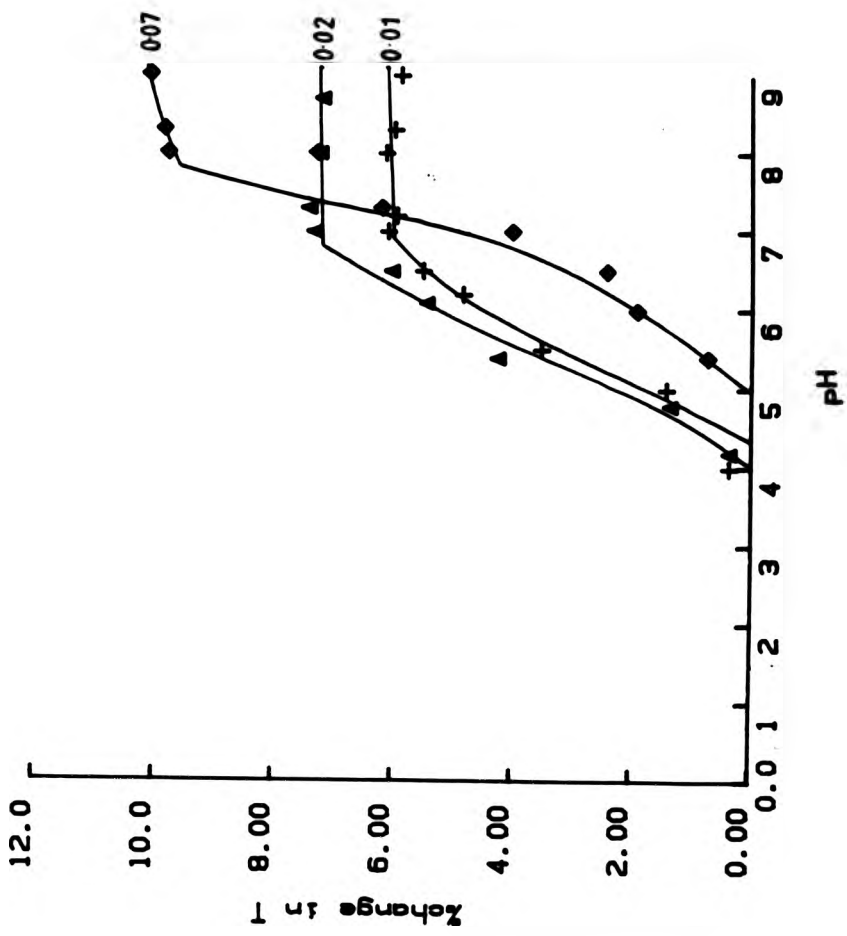


Figure 3.8 The percentage change in T as a function of pH for samples at three concentrations of the 1-2 micron size fraction

These results show that the pH at which magnetically induced orientation affects the transmitted intensity can be clearly defined. The results can be interpreted as showing the transit from face-to-edge flocculation to a stable system of discrete particles, as the charge on the initially positive edge approaches zero, at pH~7. The higher pH required to achieve this stability at the higher volume fraction of 0.07 is considered to be a concentration effect since the height of the potential barrier to flocculation (figure 1.3) decreases as the average particle separation decreases. As the concentration is increased therefore an increasingly negative edge charge is required to retain the same barrier height.

3.7 Variation of the transmittance change with  
Dispex concentration

Experiments were carried out in order to investigate the effect of surfactant concentration on the optical properties of kaolinite dispersions. The samples were prepared with Dispex concentrations in the range 1% to 4% by dry weight of clay and a pH adjusted to 8. The sample volume fraction was 0.04. The results are shown in figure 3.9

It is seen that there is a Dispex concentration for maximum transmittance change, indicating a minimum floc size. In terms of dispersion rheology the effect of Dispex on floc stability is not clear(44). However it is thought that the Dispex molecules attach themselves to the particle surface and sterically hinder aggregation as discussed in chapter 1. The Dispex concentration at which the maximum

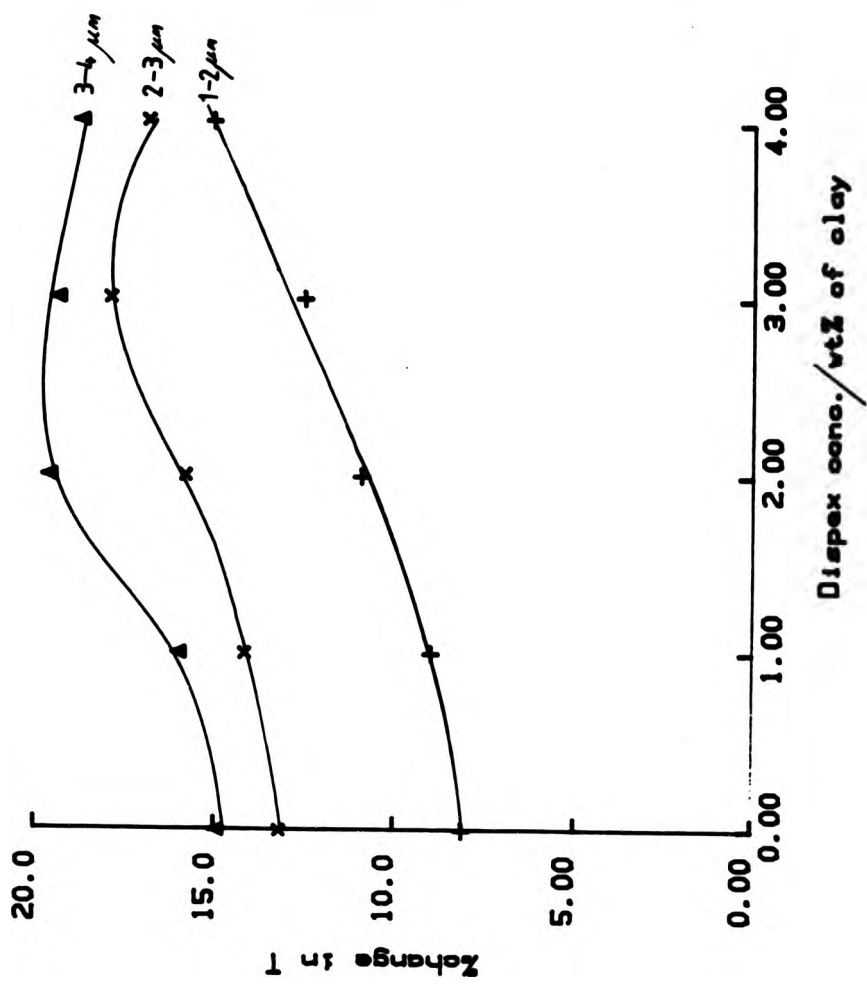


Figure 3.9 The percentage change in T as a function of Dispex concentration for three kaolinite size fractions

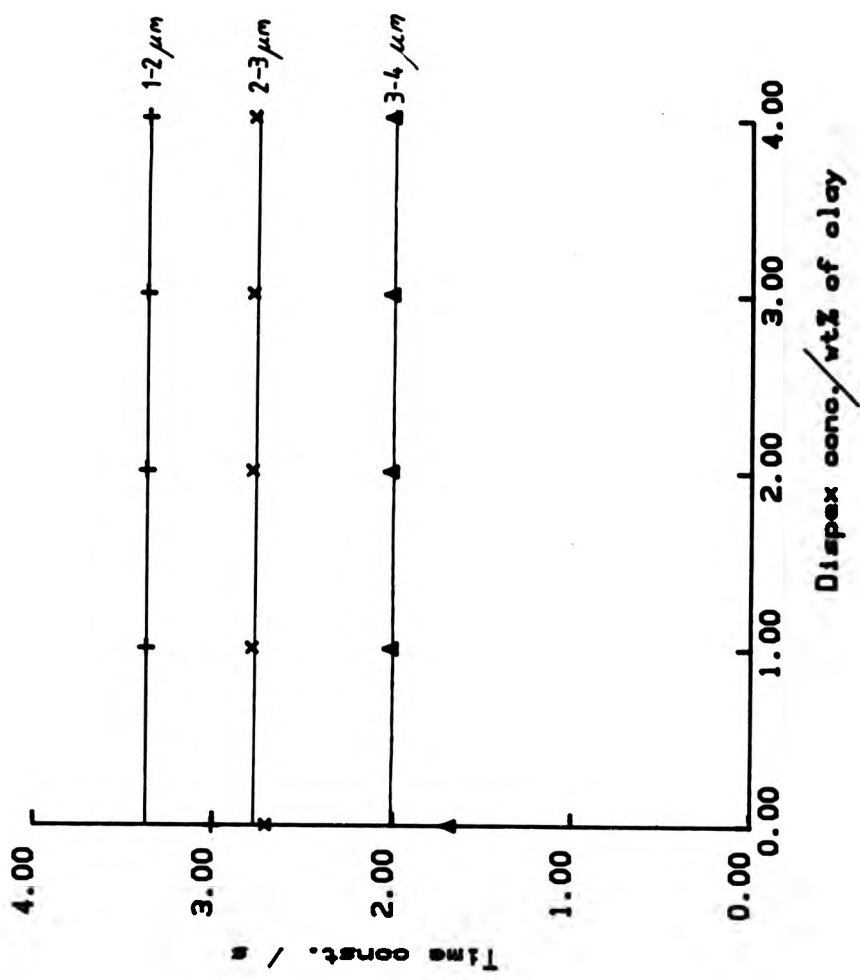


Figure 3.10 relaxation time as a function of Dispex concentration for three kaolinite size fractions

percentage change occurs is clearly dependant on the particle size, or perhaps more importantly the total sample surface area which for a given concentration increases with decreasing particle size. This is likely since the Dispex molecules are surface agents.

The decrease in percentage change after the maximum is reached indicates reflocculation. This may be due to calcium bridging, or due to electrostatic instability. These two effects have been discussed in chapter 1.8. Gregory(51) has shown that *polymer* bridging will only take place in kaolinite dispersions when calcium is added, e.g. by preparing the samples in tap water, desorption of calcium from the particle surface(34) if it occurs is not sufficient. Since the dispersions used here were prepared in de-ionised water reflocculation is unlikely to be due to this mechanism.

Dispex donates sodium ions to the dispersion hence increasing the electrolyte concentration, eventually this will produce electrostatic instability and face to face flocculation, since Dispex will still provide a steric repulsive force hindering edge to edge and edge to face flocculation. This is thought to be the mechanism responsible.

The increase in the transmittance change with particle size is interpreted as an increase in the field induced particle orientation, since the interparticle separation is increased for the same concentration, as the particle size is increased and the particles have more free volume in which to align in the field.

3.8 Variation of relaxation time with Dispex concentration and particle size

Relaxation time with particle size was investigated for three particle sizes at a volume fraction of 0.04.

The results are shown in figure 3.10.

They indicate that the relaxation process is independent of Dispex concentration over the kaolinite concentration range used. These data can be interpreted to mean that Dispex increases the number of optically anisotropic particles or flocs but not their size and at low kaolinite concentrations, the addition of Dispex does not significantly increase the dispersion viscosity.

For single particles relaxing under Brownian motion the relaxation time decreases with particle size. Here this is not the case, relaxation time increased as the particle size decreased. This data can be explained in terms of coupling between rotational and translational Brownian motion. If the time required for rotation is commensurate with the mean free time for interparticle collisions the rotation will be hindered and the relaxation time increased. The average separation  $d$ , between spheres of diameter  $ESD$ , at a volume fraction  $v$ , is given by

$$d = (v^{-1/3} - 1)ESD. \quad (3.16)$$

This gives a value of about 2  $ESD$  for the volume fraction used here, this is thought to explain the data.

## CHAPTER 4

### Ultrasonic orientation

#### 4.1 Introduction

The use of an ultrasonic field to orient the non-spherical kaolinite particles is described in this chapter.

The disc shaped kaolinite particles are thought to be oriented by a torque acting to reduce the angle between the disc normal and the ultrasound propagation direction, as in the behaviour of the Rayleigh discs [45].

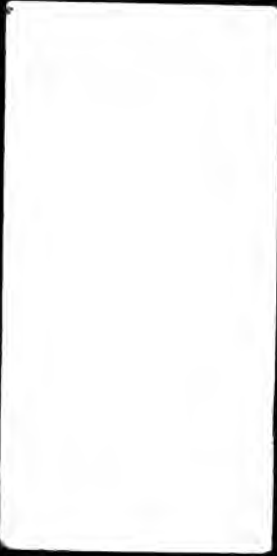
Initial experiments were carried out in an attempt to gauge the usefulness of ultrasonic orientation in colloid-optical research.

#### 4.2 Apparatus

A Scisonics pulse generator was used as the power source to deliver a 5ns, 150V pulse to a Scisonics PZT ultrasonic transducer. The pulse repetition frequency could be varied between 1 kHz and 10 kHz. It was found that the maximum repetition frequency (i.e the maximum time-average acoustic power) produced the maximum orientation, as measured by the optical reflectance change which increased approximately linearly with repetition frequency. Complete orientation was not achieved with the available energy input.

When the 5ns pulse is applied to the transducer the transducer rings at its resonant frequency of 5 MHz with a decaying amplitude for approximately 20 cycles. The transducers used were mounted in a stainless steel cylinder packed with an acoustically matched black epoxy resin. For the experiments which measured the acoustic properties of





the kaolinite samples, the sample cell consisted of two transducers (a sender and a receiver) situated at either end of a PTFE tube. Located towards the centre of this closed cell a notch was cut out to allow access for filling and cleaning. The cell path length was fixed at 9mm. This apparatus is shown schematically in figure 4.1.

For the opto-acoustic measurements a PTFE tube was fixed around a transducer, such that the top of the transducer acted as the bottom of a reflectance cell. The absorbing black epoxy resin giving a small but finite reflectance at zero path length. The light source used was derived from a tungsten lamp powered by a Farnell stabilised power supply.

The bifurcated fibre used here had a diameter of 3mm. The sample arm of the fibre was in direct contact with the sample thus avoiding unwanted window corrections as discussed earlier. The output end of the fibre illuminated a  $1\text{cm}^2$  silicon detector, the output from the detector was amplified and displayed by a Macam photometer. Finally the photometer output was monitored by a BBC microcomputer. The apparatus is shown in figure 4.2.

#### 4.3 Experimental procedure

In the acoustic experiments the transmitted sound intensity was detected using a 10 MHz oscilloscope. The error in taking amplitude measurements from the oscilloscope was of the order of 5%. Attempts were made to measure the sound velocity variation with concentration but with little success. Urlick [46] reports that for the volume fraction range up to 0.4 the variation of sound velocity with

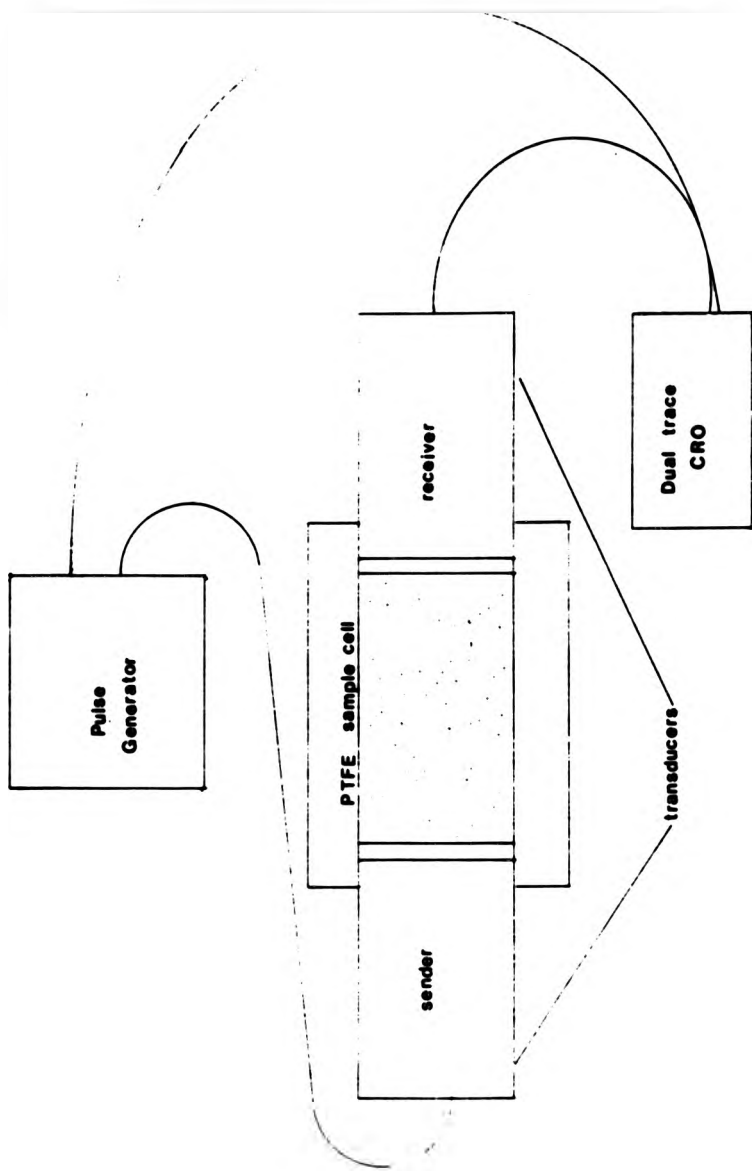


Figure 4.1 Schematic of the apparatus used in the Ultrasonic transmission experiments

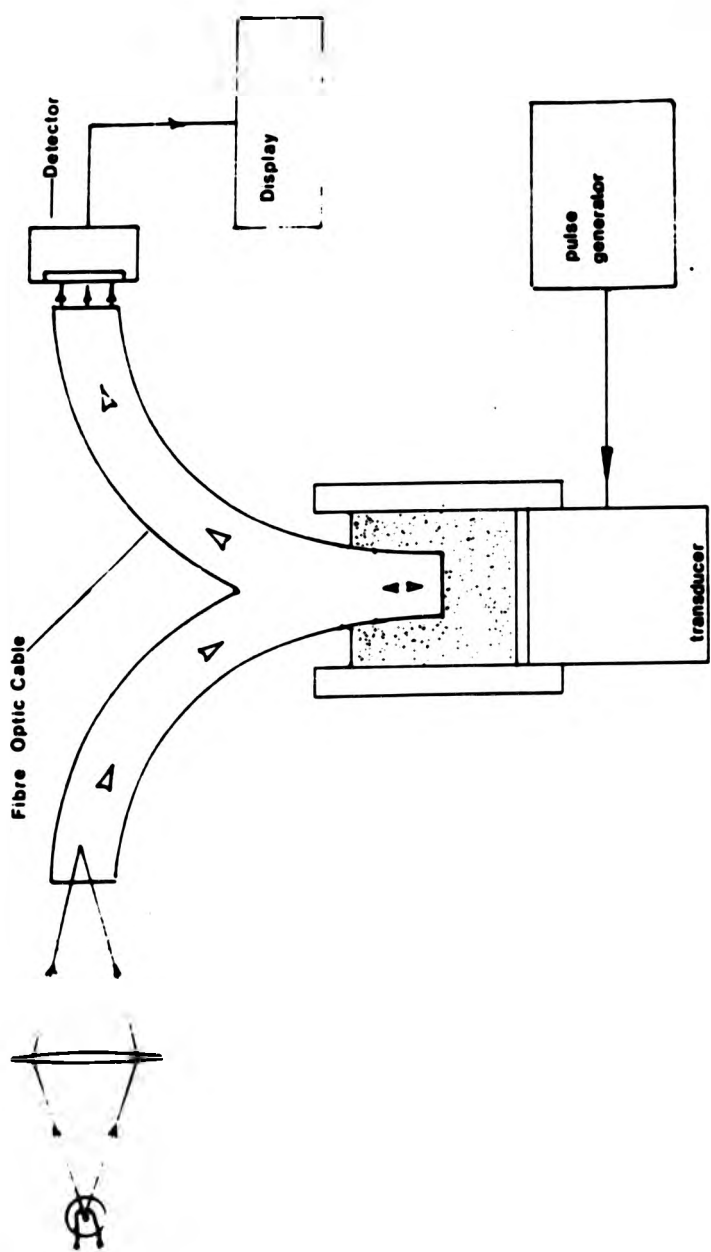


Figure 4.2 Schematic of the apparatus used in the opto-sonic experiments

concentration is of the order of 3%.

For the opto-sonic experiments, after the samples were placed in the cell the sample end of the fibre was fixed in its mount and the path length adjusted.

Before each data run the sonic field was applied until the reflectance reached a steady value then a computer programme was initiated to follow the decay of the reflectance with time after the field was removed.

#### 4.4 Variation of the transmitted ultrasonic intensity with concentration

Using the acoustic cell the transmitted ultrasonic intensity relative to that of water was measured using the oscilloscope. Samples in the volume fraction range 0.02-0.14 were prepared as described in chapter 1 with a pH fixed at 8 and without the addition of Dispex.

Attenuation of high frequency sound waves has been shown by Stokes[47] and Kirchhoff[48] to be due to viscous drag and heat conduction, assuming no scattering.

The transmitted ultrasonic  $T_u$  intensity falls by a factor  $\exp(-2ax)$  after a traversing a distance  $x$ . The quantity  $2a$  is the intensity absorption coefficient given by

$$2a = \frac{4\pi^2 f^2}{c^3 \rho} \left[ \frac{4}{3} \eta + \frac{(k-1)}{c_p} \eta \right] \quad (4.1)$$

where  $\rho$  is the mean density,  $\eta$  is the viscosity,  $f$  the frequency,  $c$  the velocity of sound in the medium,  $k$  the ratio of the specific heats,  $c_p$  the specific heat at constant pressure and  $k$  the thermal conductivity.

For kaolinite dispersions the heat conduction term is negligible. Beazley [49] reports that the variation of the

shear viscosity of kaolinite dispersions measured at high velocity gradients increases approximately linearly with volume fraction over the concentration range used here.

Taking logs (Ln) and writing  $1000(1+1.6v)$  for the mean density, and  $(1+bv)$  for the relative viscosity at a volume fraction  $v$  we have

$$\ln \frac{T}{\rho} = A \frac{(1+bv)}{(1+1.6v)} \times \quad (4.2)$$

here the path length  $x$  is 9mm.

A non-linear data fitting programme was used, fitting the experimental values of  $T$  and  $v$ . The data and the fitted function are shown in figure 4.3 and show good agreement with the form of the equation. The value of the proportionality constant  $b = 3.8$ , is a factor of 5 lower than the value obtained from the data presented by Beazley[49]. This can be interpreted in terms of the frequency dependance of the viscosity.

These results clearly suggest that attenuation in deflocculated dispersions of kaolinite is due to viscous drag and not to scattering. This is to be expected since deflocculated kaolinite particles are much smaller than the ultrasonic wavelength of 0.3mm.

#### 4.5 Variation of the transmitted ultrasonic intensity with pH

With the fixed path length 9mm acoustic cell the transmitted ultrasonic intensity was measured for samples prepared as in chapter 1 with a volume fraction of 0.10 and a pH in the range 3 to 10. The results are shown in figure 4.4 with the transmitted sound intensity in arbitrary

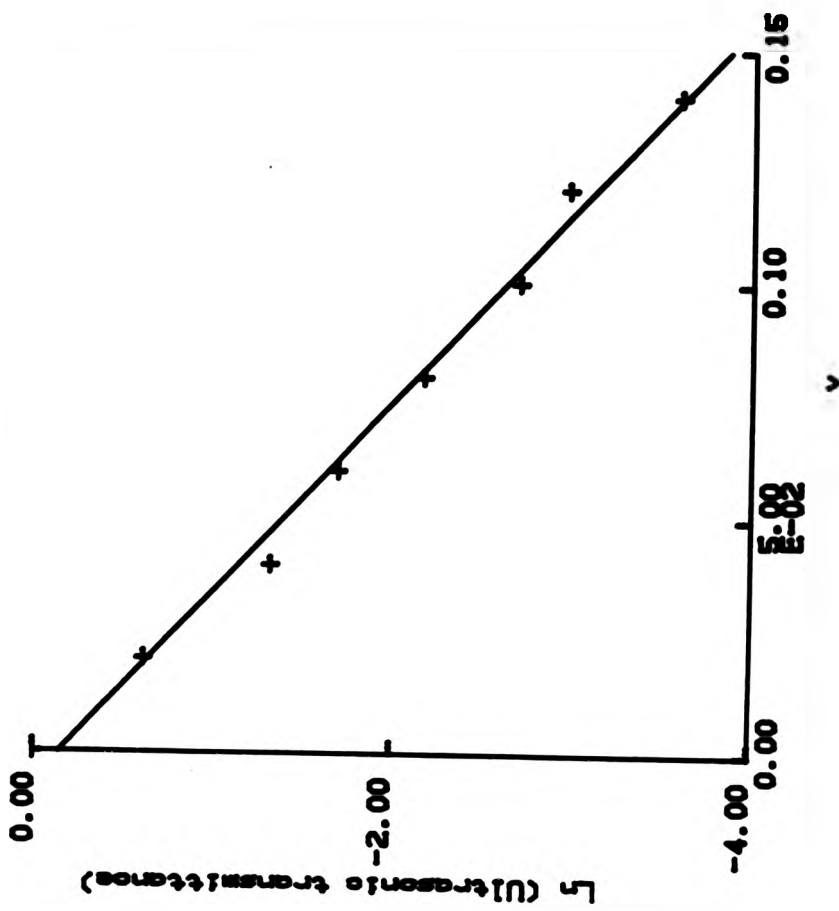


Figure 4.3 Ln Ultrasonic Transmittance as a function of dispersion volume fraction  $v$  for SPS. The solid line is obtained from the Stokes-Kirchhoff equation (4.1) for acoustic absorption

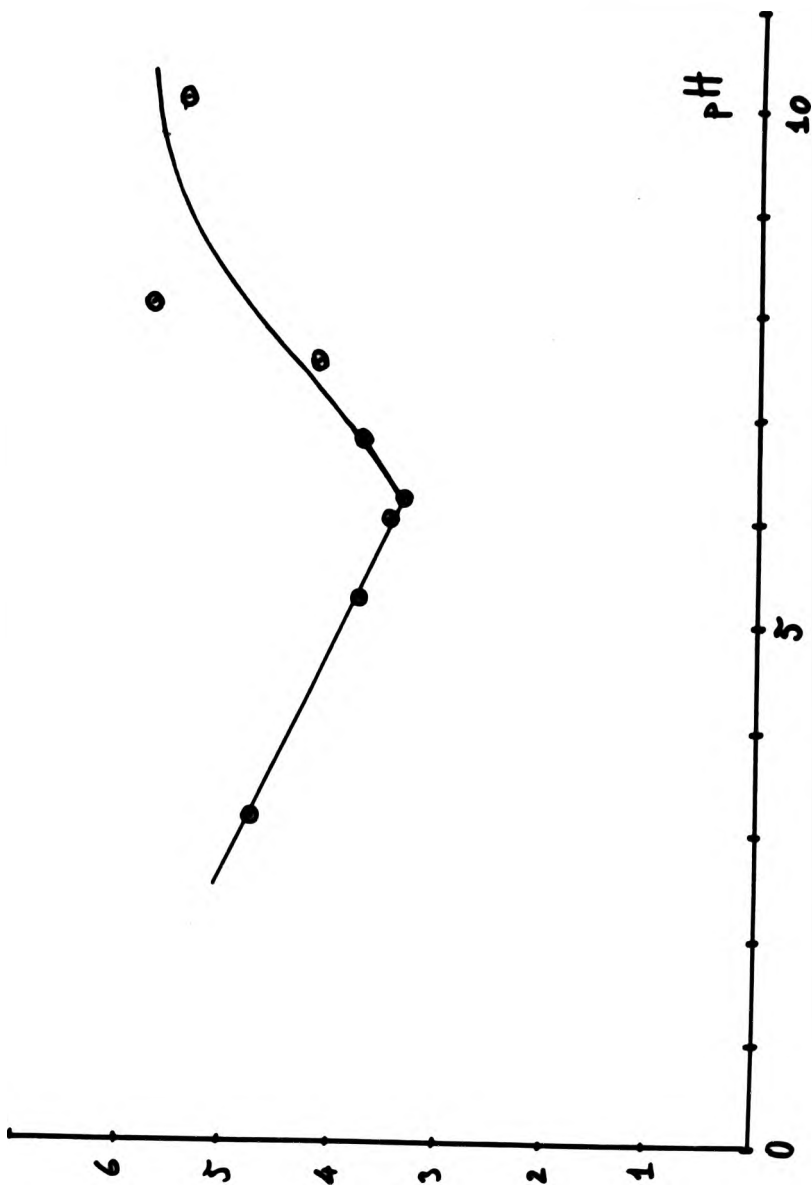


Figure 4.4 Ultrasonic transmittance (in arbitrary units) as a function of pH for a dispersion of SPS at a volume fraction of 0.1

units. These results can be interpreted as evidence of sonic resonance analogous with its optical counterpart. It is known that increasing the pH of a kaolinite dispersion decreases the floc size. The scattering of the sound waves will become marked when the floc size is commensurate with the wavelength. For the transducer used the wavelength of the sound waves in water is 0.3mm which therefore suggest flocs of a similar size at pH6.

4.6 Variation of reflectance change  
with path length

Differentiating equation 1.5 we find the fractional change in R to be given by

$$dR/R = dS/S [1/(1+Sz)] \quad (4.3)$$

for a path length z, indicating that the fractional change in R will decrease with concentration.

These experiments were carried to test the validity of equation 4.3.

The sample used was of volume fraction 0.002 with a pH adjusted to 8.

The results are shown in figure 4.5.

It was thought that the initial increase in the reflectance change with path length was due to acoustic interference at path lengths commensurate with wave train length, reducing the intensity of the progressive wave part of the acoustic field. However at short optical depths, (i.e. for a volume fraction of 0.002 path lengths less than 10mm), the static reflectance of the sample is equal to or less than the reflectance of the cell. Therefore the fractional change



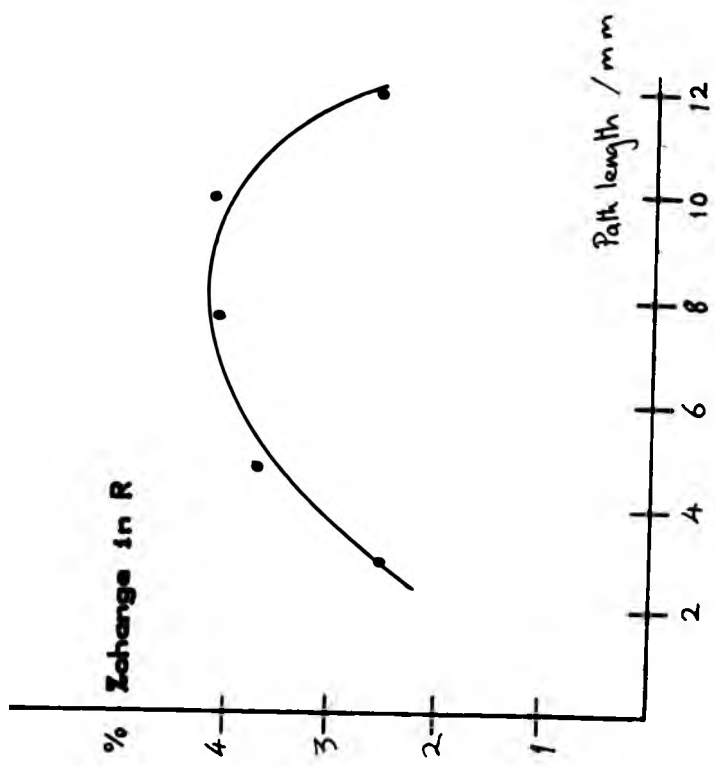


Figure 4.5 The percentage change in reflectance R as a function of path length for a dispersion of SPS at a volume fraction of 0.002

in reflectance as measured is less than the true value by a factor of  $R/(R+C)$  where  $C$  is the cell reflectance and  $R$  is the sample reflectance. This behaviour accounts for the initial rise in the reflectance change, beyond path lengths of 10mm the reflectance change decays as expected. For strongly multiple scattering dispersions  $R \gg C$  for all path lengths greater than 0.1mm, the shortest path length used.

#### 4.7 Variation of reflectance change with concentration

These experiments were carried out in order to clarify the results in 4.6 to investigate whether the initial rise in reflectance with path length, observed previously, is due to the cell reflectivity or acoustic interference. The experiments were conducted with a fixed path length of 5 mm which clearly limits the concentration range over which measurements could be made since for large optical depths the reflectance reaches saturation i.e the optical efflux is equal to the influx and therefore orientational effects cannot be observed optically. The volume fraction range used was from .002 to 0.01 with the pH fixed at 8 for all samples. The results are shown in figure 4.6. For a fixed path length the variation of the fractional change in the reflectance will depend on the scattering parameter  $S$ , the fractional change in  $S$  and the intensity of the sound field. From figure 4.3 it can be seen that the intensity of the sound field varies by only a few percent over this concentration range and since the variation in the optical response is expected to be of the order of 30%, it is

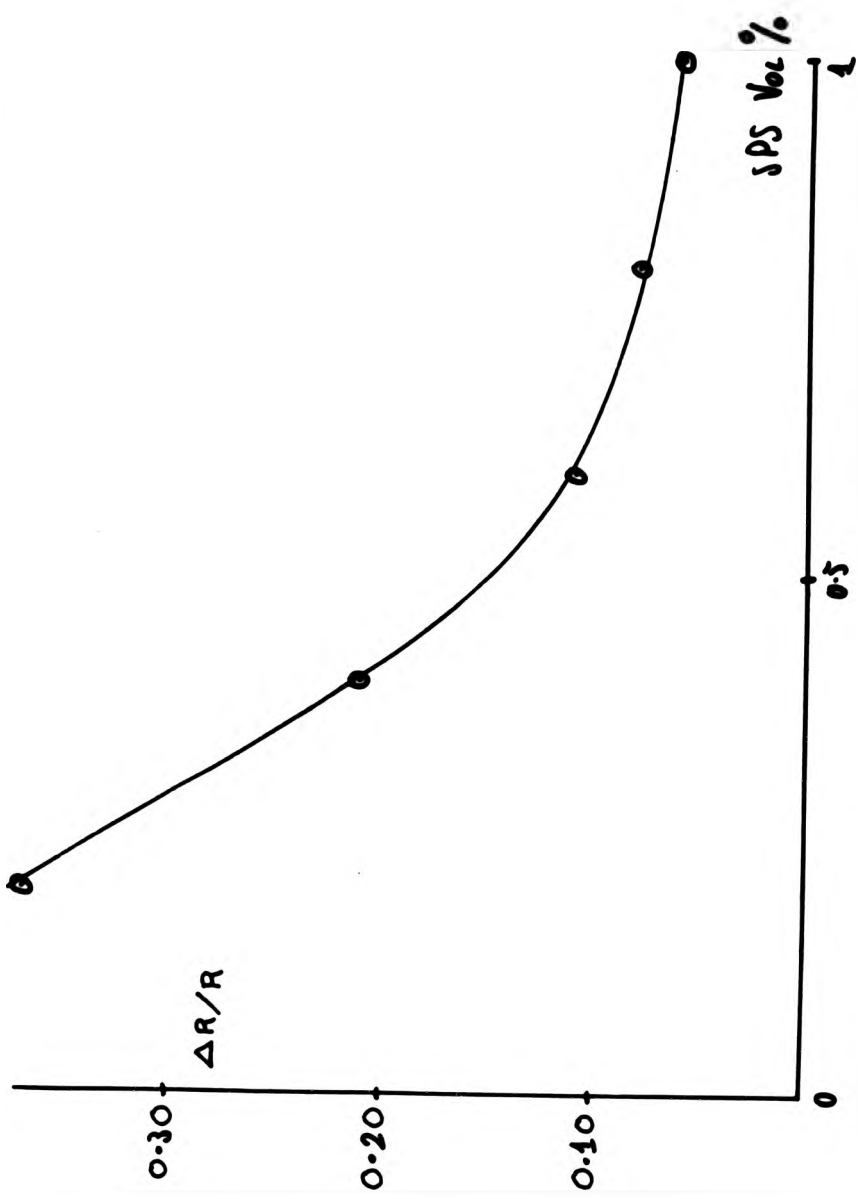


Figure 4.6 the fractional change in R as a function of volume fraction for dispersions of SPS

concluded that this behaviour is due to an optical effect.

#### 4.8 Variation of reflectance change with pH

Samples with a fixed volume fraction of 0.008 and pH in the range 6 to 10 were prepared as described in chapter 1, with the path length fixed at 5mm. The results are shown in figure 4.7.

These results indicate that an opto-ultrasonic system can be used as a means for monitoring flocculation.

It is known that flocculation within a colloidal dispersion is extremely pH dependant and in the case of kaolinite it is also thought that particles flocculate in a face to edge mode such that flocs appear optically isotropic and therefore orientation does not change the optical scattering properties of the flocs. It is also known that above a pH of 7 the dispersion becomes deflocculated so that orientation will produce a reflectance change.

#### 4.9 Conclusion

The experimental results suggest the usefulness of using acoustic and opto-acoustic techniques to characterise dispersions of non-spherical particles. From this brief examination it is apparent that a greater time averaged acoustic intensity is required to obtain maximum particle orientation.

The concentration range over which opto-acoustic measurements can be made can be greatly extended simply by reducing the path length.

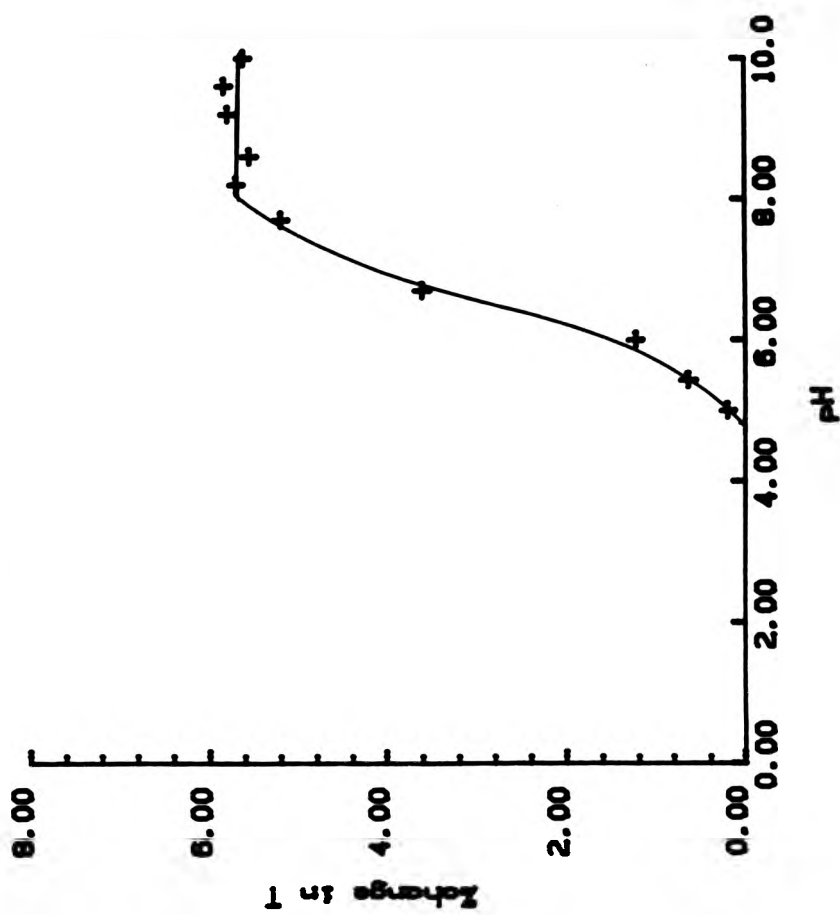


Figure 4.7 The percentage change in R as a function of pH for a dispersion of SPS at a volume fraction of 0.008

## CHAPTER 5

### Shear-induced orientation

#### 5.1 Introduction

Non-spherical particles in shear flow are subject to the orienting influence of the hydrodynamic field and the disorienting influence of Brownian motion. Therefore there is a change in orientation from random to shear-oriented. This shear orientation will decay to random orientation when the hydrodynamic field is removed, by the action of rotary Brownian motion. In the case of kaolinite dispersions, it is possible to follow this micro-rheological behaviour optically.

#### 5.2 Apparatus

The apparatus used in this series of experiments is shown schematically in figure 5.1.

A tungsten lamp powered by a Farnell L12-10C power supply provided the light source used.

A Macam 400-700nm strip spectrum filter with a 14nm half-height halfwidth was used to vary the wavelength of the incident light.

The incident light was delivered to the sample through a bifurcated fibre optic cable of 3mm radius. The reflectance was detected by a Macam silicon photodiode ( $1\text{cm}^2$ ) through the return arm of the fibre optic cable. The response curve of the fibre used is shown in figure 5.2.

The sample cell consisted of an 11mm radius glass cylinder, 26mm in height, which was fixed upon a matt black plastic

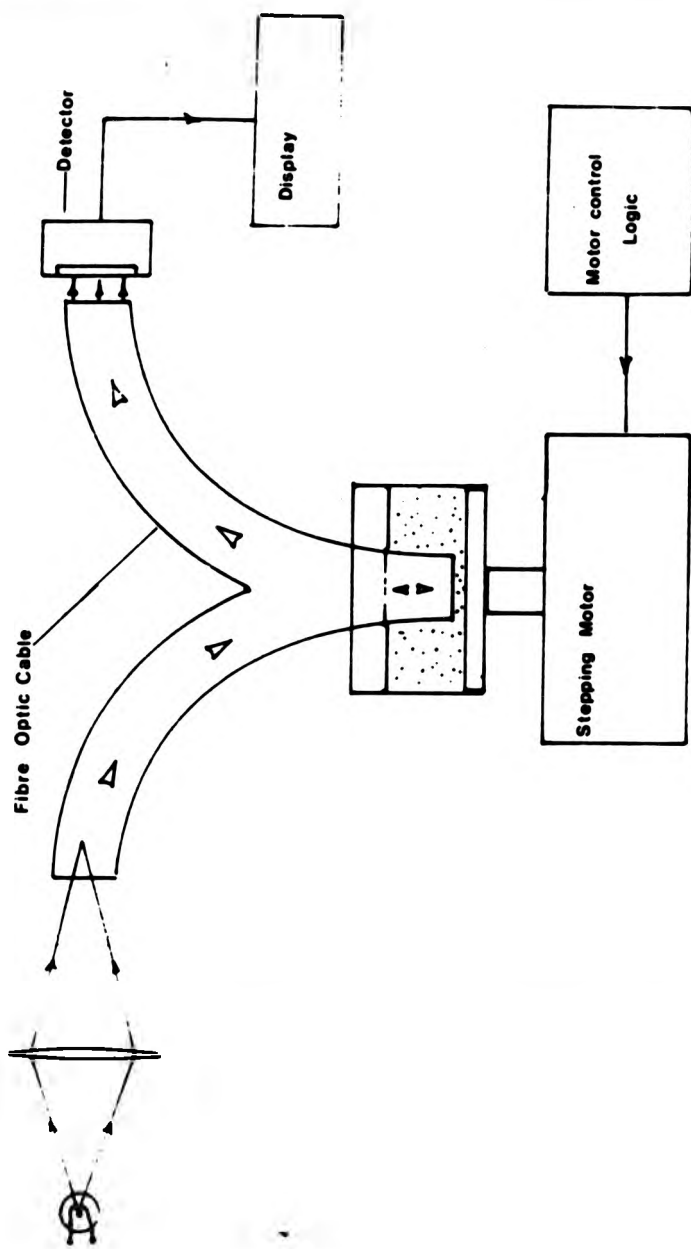


Figure 5.1 Schematic of the shear-optical apparatus

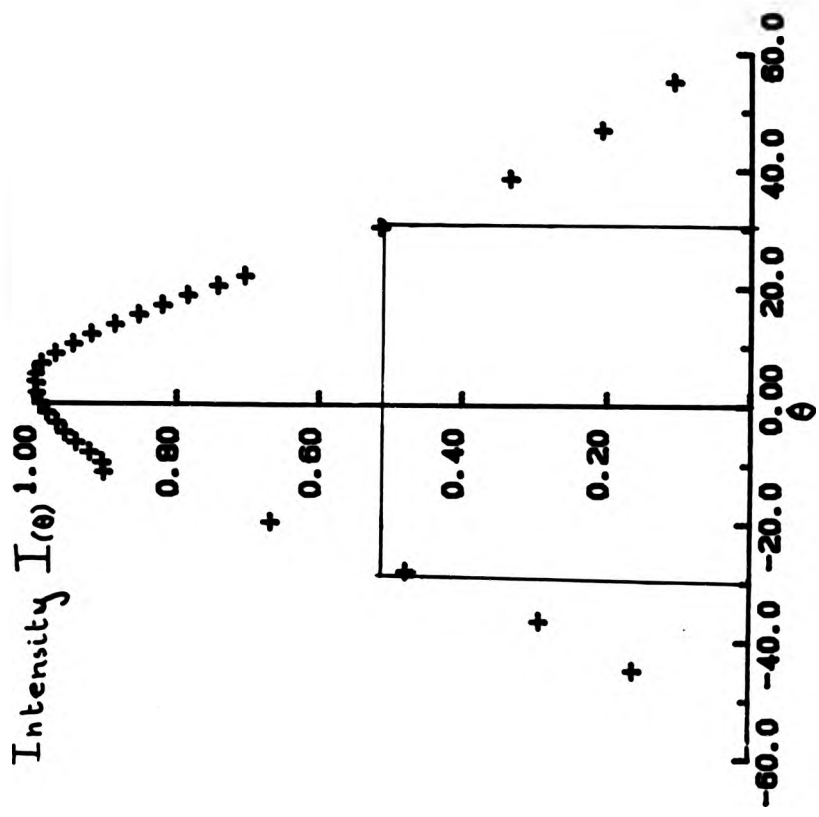


Figure 5.2 Optical response of the fibre optic bundle as a function of angle of incidence defining the numerical aperture as 0.5 ( $\sin 30^\circ$ )



base-plate. The cell was mounted coaxially on the spindle of a 1.8 degree stepping motor (i.e. 200 steps per revolution), which was driven by a power supply controlled by a (.001-1000)Hz square wave signal generator.

The output from the photodiode was displayed on a Macam 3000 photometer, which also amplified the signal. An analogue output from the photometer was monitored by a BBC microcomputer via its analogue to digital converter.

With the present apparatus the velocity gradient  $G$  at a distance  $a$ , from the bundle centre is given by

$$G = \frac{aw}{d} \quad (5.1)$$

where,  $w$  is the angular frequency of the stepping motor and  $d$  is the optical path length. The average velocity gradient  $\langle G \rangle$  is given by the area weighted average of  $G$

$$\langle G \rangle = \frac{\int_0^r 2wa^2 da}{\int_0^r 2a da} = \frac{2}{3} \frac{wr}{d} \quad (5.2)$$

where  $r$  is the bundle radius.

Thus  $\langle G \rangle = 2/3 G(\max)$ , where  $G(\max)$  is the velocity gradient at  $r$ .

### 5.3 Initial experiments

Experiments were carried out to minimise the effects of vibration and turbulence.

Initially the apparatus was mounted on a single optical bench. This led to a high noise (random signal) level due to vibrations from the stepping motor which were transmitted along the optical bench to the pinhole. To reduce this noise level the optical system was adjusted to produce an out of focus broad image at the input arm of the bifurcated fibre. The dynamic components were mounted on a

separate optical bench which in turn was mounted on soft rubber feet. The combination of these improvements reduced the noise/signal ratio to  $< 0.1\%$  for a white light source. When the filter was used the apparent noise/signal level increased due to the detector characteristics and the considerable reduction in optical flux. Here the noise level was  $< 0.3\%$  for all wavelengths above 450nm and at 400nm the noise level was  $< 0.5\%$ . It was decided that these levels were acceptable in view of the several % change in reflectance on shear.

In the shear system used, see figure 5.1, the critical Reynolds number, below which the flow is laminar, is not easy to determine theoretically. However there are empirical indicators of the onset of turbulent flow. The fluid adjacent to the base of the cell experiences a centrifugal force which causes a secondary flow in the radial direction. There are corresponding centrepetal flows in the fluid close to the stationary fibre and the top of the fluid column.

A flow visualisation experiment, figure 5.3, using a laser beam and stroboscope, was conducted to observe the onset of these secondary flows. It was found that they could be minimised by using a 3mm radius cable instead of the 1.5mm cable used in the static experiments reported in chapter two, (thus doubling the average velocity gradient for a given angular velocity and path length), and by fitting a 9mm radius collar around the end of the sample arm of the fibre in order to reduce the secondary flows. These improvements allowed for non-turbulent shear in the

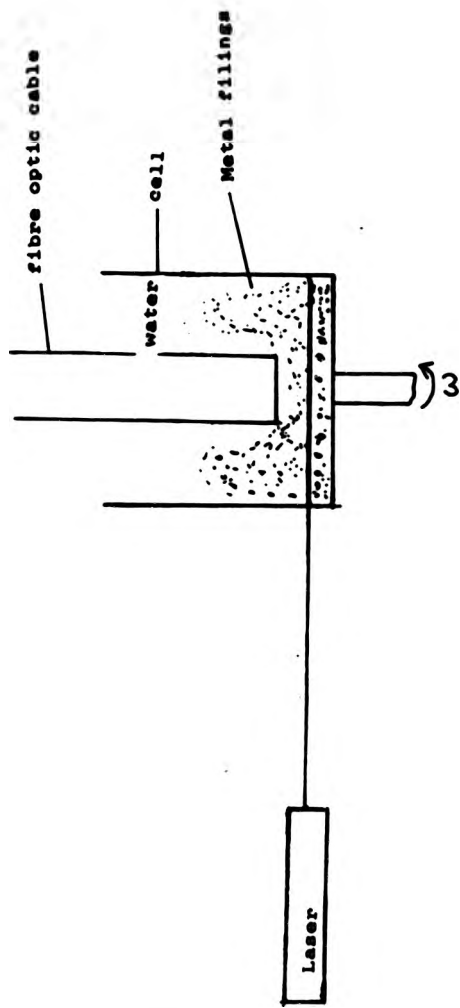


Figure 5.3 Schematic of the flow visualisation experiment allowing the onset of turbulence to be observed

velocity gradient range upto  $80s^{-1}$

Having made the foregoing improvements to the experimental system, an experimental procedure was needed to minimise the effects of settling. When settling took place the static reflectance increased over time due to the increased concentration in the illuminated volume i.e particles from the non-illuminated dispersion above the fibre settled into the illuminated volume. To overcome this it was decided to thoroughly mix the samples prior to taking experimental data as described below. Figure 5.4 shows general graphs of the change in reflectance with a fixed velocity gradient  $G(\max)$ . Graph 2 represents idealised behaviour where there is no apparent effect caused by settling. Graph 3 represents the case where settling occurs prior to the experiment, the reflectance decreases with time for a constant velocity gradient. The reflectance reaches a steady value when the sample is eventually homogenised by the mixing effect of rotation. In the absence of the field the reflectance decays until settling once again becomes dominant. To overcome the problem of settling it was decided to mix the samples using a high angular velocity and then switch to the required angular velocity before each data run. It was found that reproducible results were achieved when samples were mixed using a high angular velocity, producing turbulent flow, for a period of 30s. Therefore the following experimental procedure was adopted. After mixing, the velocity gradient was switched to that required, the reflectance was allowed to decay to a steady value before a data run was initiated. On each data run

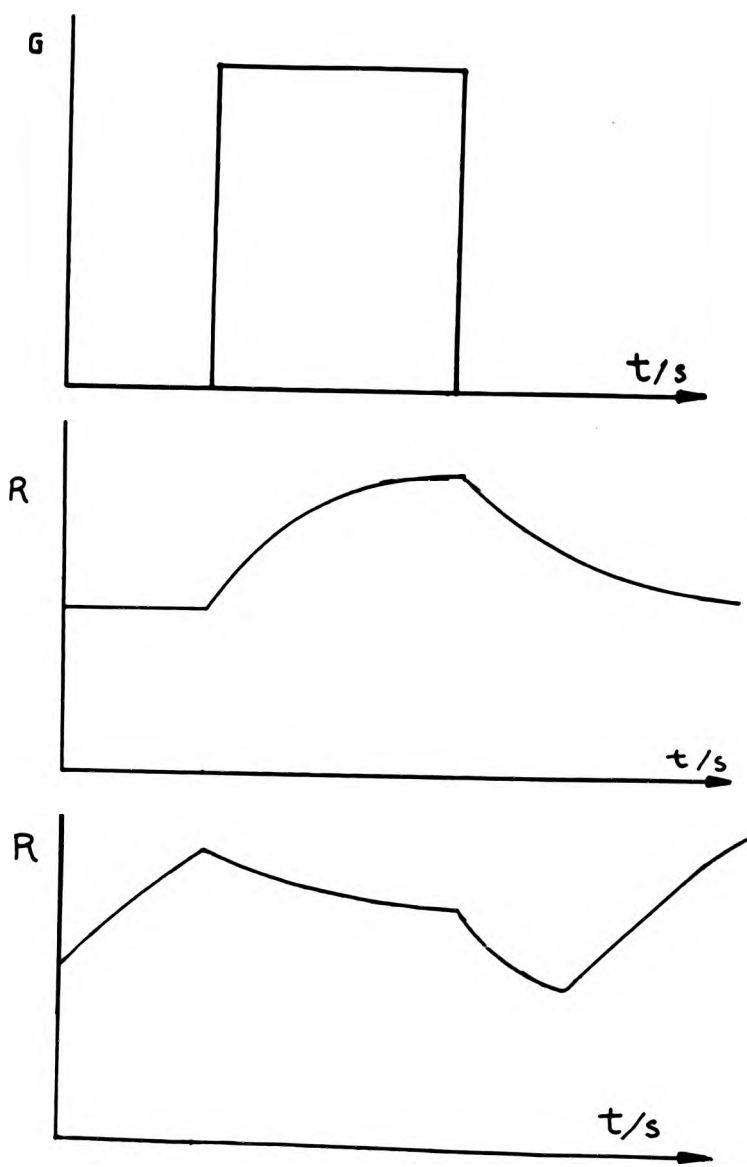


Figure 5.4 generalised plots of the percentage change in  $R$  for different degrees of settling

after the reflectance had reached a steady value the data acquisition programme was initiated. The field was removed approximately 5s into the run in order to check that the reflectance for a constant field was also constant. Using this approach it was found that for all particle sizes below 3 microns settling was not apparent.

At this stage it was then possible to proceed with the following experimental investigations.

#### 5.4 Variation of reflectance with velocity gradient

In the group of experiments to be described here the path length, (i.e. the separation of the sample end of the fibre optic cable from the bottom of the sample cell), was fixed at 0.3mm. An alternative approach would be to conduct experiments with the path length varied to give a fixed reflectance, for random orientation, for all particle sizes used. The former approach was used because of the problem of settling discussed above.

The light source was used without the filter so as to give the lowest noise level in order to resolve reflectance changes at low velocity gradients. The samples were prepared as described in chapter 1 with a kaolinite volume fraction of 0.09. Dispex was not added and the sample pH was fixed at 8. Data were obtained for the following ESD size fractions (given in microns) 0.4-0.5, 0.5-0.6, 0.6-0.7, 0.7-0.8, 1-2. The results are shown graphically in figures 5.5-5.9 respectively.

Measurements have previously been made on dilute ( $v = 0.0005$ ) dispersions of kaolinite of the shear dependant

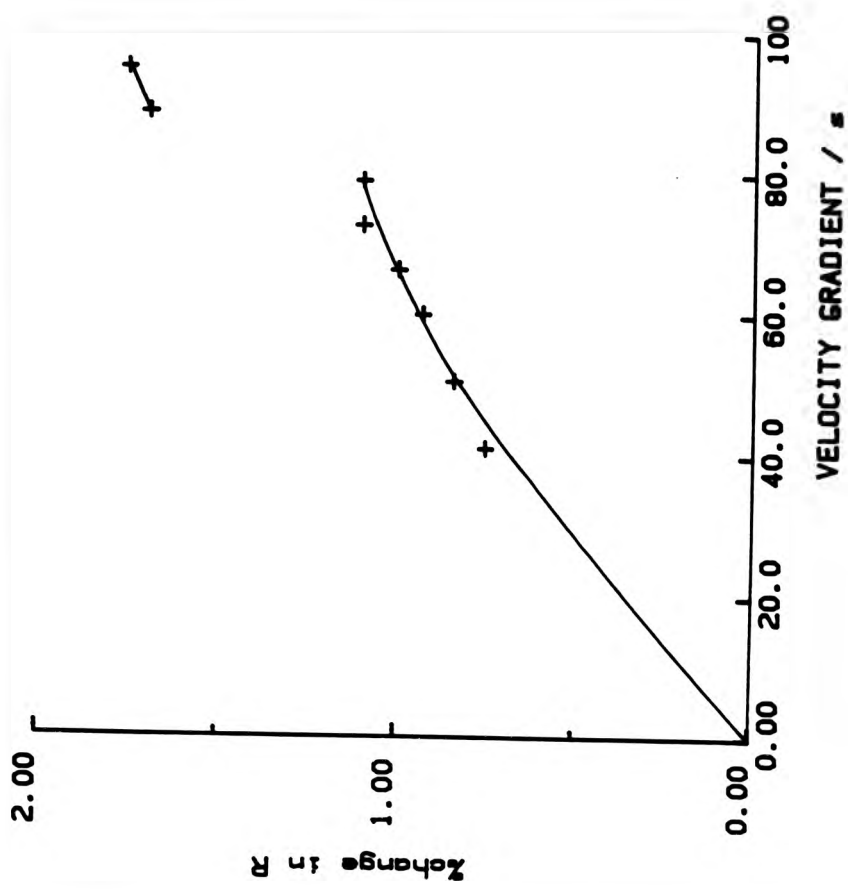


Figure 5.5 The percentage change in R as a function of velocity gradient for the 0.4-0.5 micron kaolinite size fraction at a volume fraction of 0.09

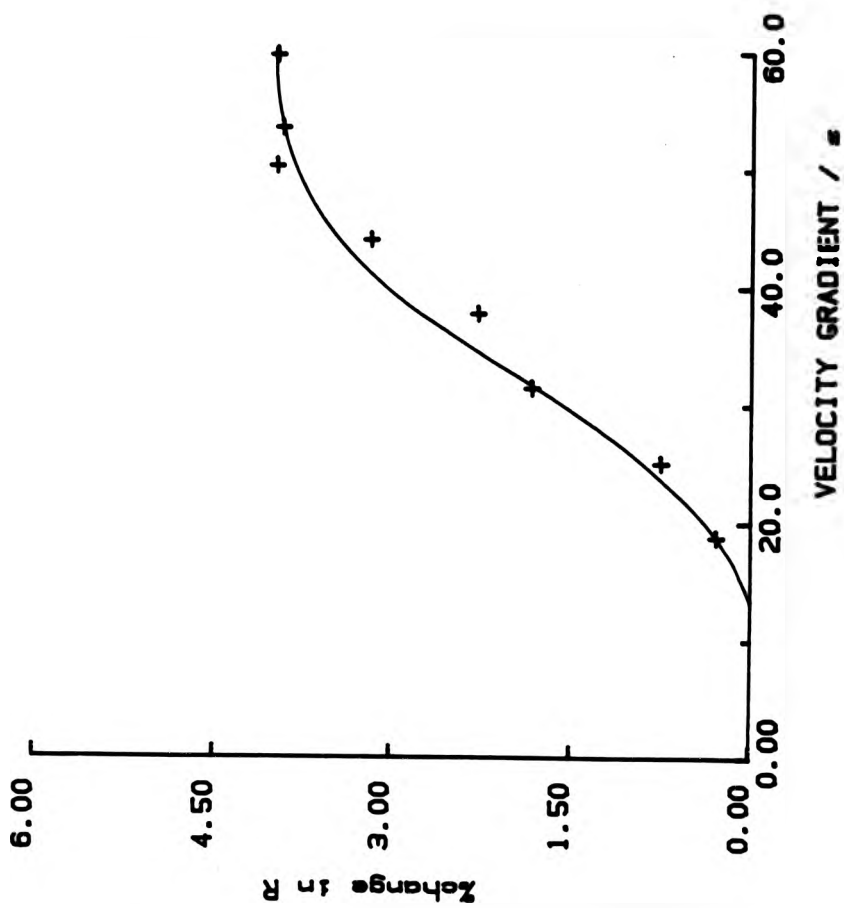


Figure 5.6 The percentage change in R as a function of velocity gradient for the 0.5-0.6 micron kaolinite size fraction at a volume fraction of 0.09



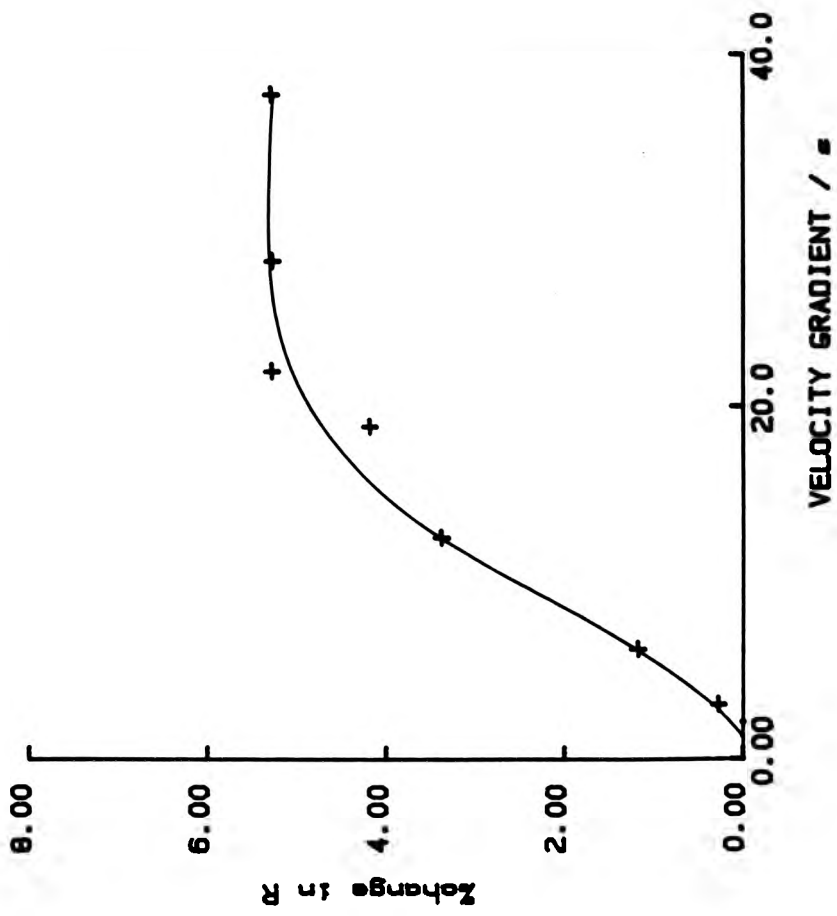


Figure 5.7 The percentage change in R as a function of velocity gradient for the 0.6-0.7 micron kaolinite size fraction at a volume fraction of 0.09

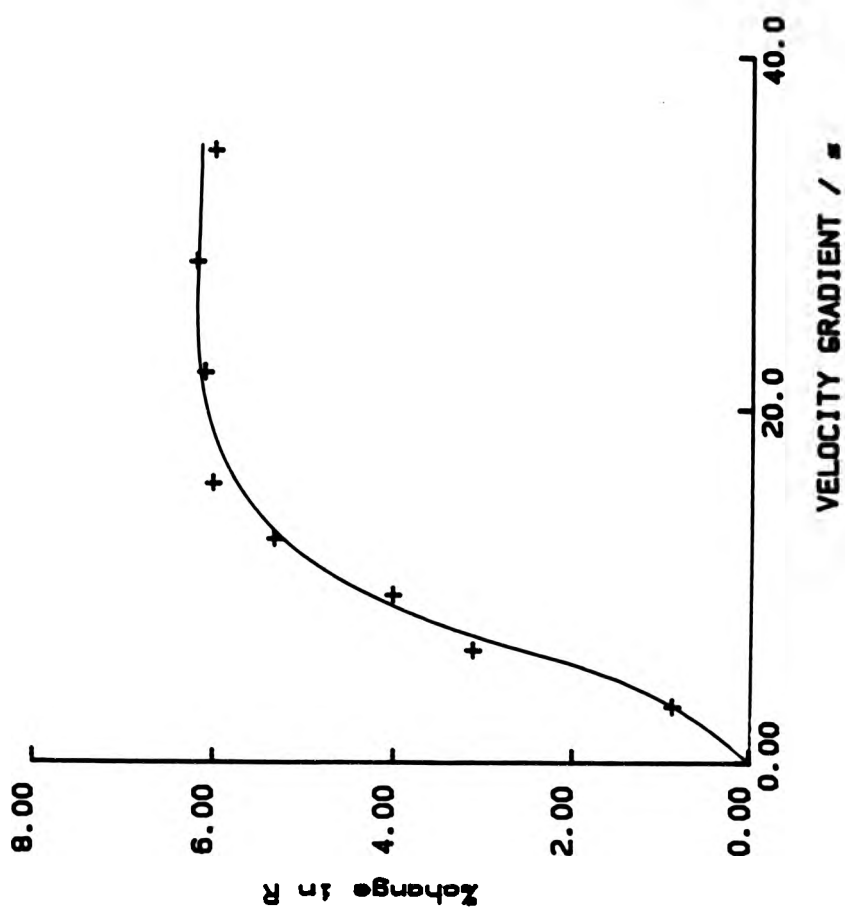


Figure 5.8 The percentage change in R as a function of velocity gradient for the 0.7-0.8 micron kaolinite size fraction at a volume fraction of 0.09

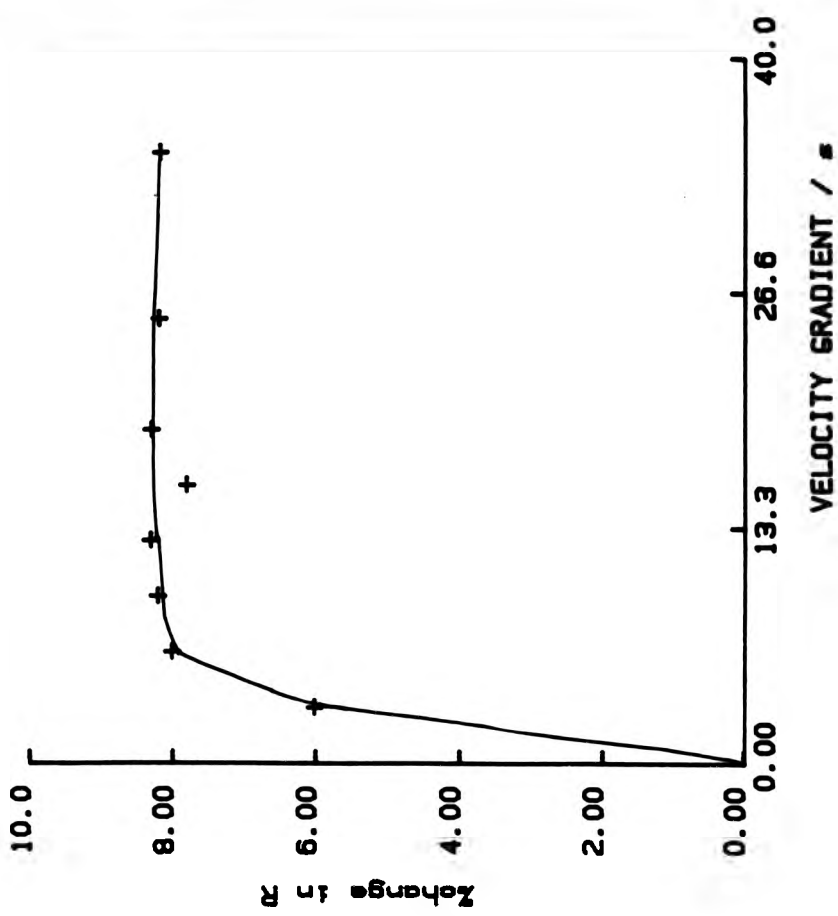


Figure 5.9 The percentage change in R as a function of velocity gradient for the 1-2 micron kaolinite size fraction at a volume fraction of 0.09

optical anisotropy[43], where the coherently transmitted intensity was measured as a function of shear rate for the same size fractions as used here with the exception of the 0.4-0.5 fraction. The data presented show the same functional form as the data here. This is taken as evidence to support the claim in chapter three that orientational information is retained when multiple scattering is the dominant mode of photon transport. In the data presented the plateau region indicates that the shear orientation is maximised. This plateau is seen to occur at lower shear rates as the particle size is increased, and in the case of the smallest particle size fraction the maximum non-turbulent shear rate with the available apparatus was insufficient to produce complete orientation. Evidence for turbulence is the discontinuity in  $R$  seen to occur at the high shear rate in the 0.4-0.5 micron data. This behaviour is expected on the basis of single particle shear orientation i.e smaller particles require higher velocity gradients to overcome the randomising influence of Brownian motion.

#### 5.5 Variation of reflectance change with wavelength

Here the Macam filter was used to vary the wavelength of the incident light in the range 400nm to 700nm. The velocity gradient  $G(\max)$  was fixed at approximately  $40s^{-1}$  for all samples used. The samples were prepared as described in chapter 1 with no Dispex, a pH of 8 and a volume fraction of 0.09. The procedure adopted here was

firstly to adjust the filter to the required wavelength, secondly, to set the photometer to a suitable gain and check the zero, and finally to execute the experimental procedure described above. Data were obtained for the following ESD size fractions 0.5-0.6, 0.7-0.8, 1-2, 2-3. The results of these experiments are shown in figure 5.10. This work has also been previously carried out[43] in a single scattering regime, there was however a much stronger wavelength dependence exhibited than in the work presented here. This must be an effect due to multiple scattering since here the concentration is a factor of about 200 times greater than in the previous work[43].

In the theory developed in chapter three the diffraction limit of the scattering cross-section was used to simplify the integration. A more realistic approach would be to use a phase function which is particle size dependant. This more rigorous treatment may explain the difference in the wavelength dependence between the single and multiple scattering results.

#### 5.6 Variation of reflectance change with Dispex concentration

A series of experiments were undertaken in order to investigate the aggregation dependence of the anisotropy of scattering cross-section of particles or flocs. Since it is known that Dispex impedes the flocculation process in kaolinite, samples were prepared using the method described in chapter 1 with Dispex concentrations in the range 0% to 3% by dry weight of clay. However here the sample pH was

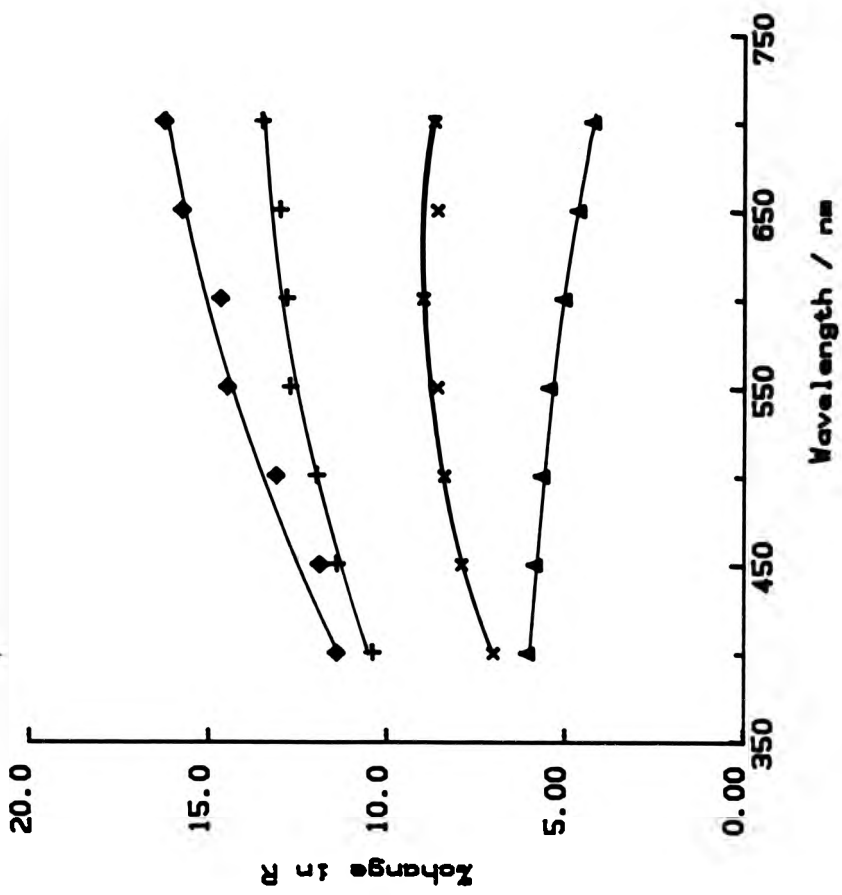


Figure 5.10 The percentage change in R as a function of wavelength for the following micron kaolinite size fractions (0.5-0.6, 0.7-0.8, 1-2, 2-3) at a volume fraction of 0.09

not adjusted externally by the addition of salt solution. The light source was used without the filter to ensure minimum noise and maximum resolution of small reflectance changes. The velocity gradient was kept constant at  $40s^{-1}$  for all samples used. The samples used were of a broad size fraction (  $80wt\% < 2microns$  ) and the volume fraction was 0.4. The results are shown in figure 5.11.

The experimental technique used here is not a true representation of the industrial process used in the de-flocculation of kaolinite slurries, but it is clear from the results that this technique can be easily adapted as a practical monitor of flocculation and de-flocculation in an industrial setting.

It should be noted that throughout this work there was no evidence to suggest that the shear fields used induced flocculation. It should also be noted that the Dispex concentration required to give the optimum signal for the shear induced reflectance change is lower than the value obtained from the magnetic work (chapter three). There are two possible causes for this behaviour. The particles under shear spend most of their time in a face-to-face orientation, therefore weak face-to-edge floccs will be broken by the aligning action of the shear field. Secondly, Dispex releases sodium ions to the solvent therefore increasing the electrolyte concentration. As the clay concentration is increased, the sodium ion concentration in the solvent is also increased for the same Dispex-to-clay concentration. Steric repulsion between a Dispex coated platelet edge and an uncoated face will

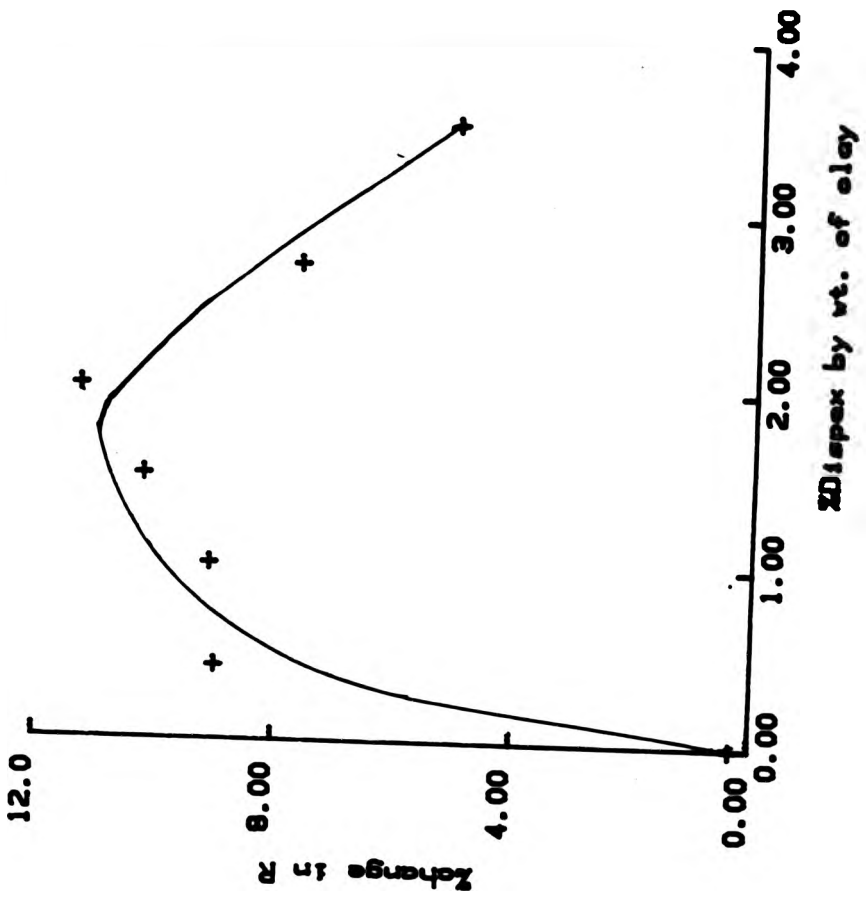


Figure 5.11 the percentage change in R as a function of Dispex concentration in a dispersion of SPS at a volume fraction of 0.1



increase the stability. Instability is increased when the sodium ion concentration begins to reduce the double layer thickness allowing van der Waals attraction between faces to dominate the electrostatic repulsive forces. There will therefore exist an equilibrium Dispex concentration for maximum stability which will vary with dispersion concentration.

5.7 Variation of reflectance change with concentration

Samples were prepared in the volume fraction range 0.05 to 0.30 with a pH adjusted to 8 and without the addition of Dispex.

The light source was used without the filter, and the path length was again 0.3mm.

The results showing the fractional change in R against concentration and the relaxation time against R are given in figures 5.12 and 5.13. The fractional change in R is deemed to be positive when the reflectance is greater with the field on. The relaxation times were taken as the time taken for the reflectance to fall to  $1/e$  of its field-on value in the positive case or to rise to  $(1-1/e)$  of its field-on value in the case when  $\Delta R < 0$ , i.e. when R decreased on applying the shear.

From the discussion on shear orientation in chapter 1 and the variation of reflectance change with velocity gradient discussed above it may be concluded that at high shear rates the disc shaped kaolinite particles are drawn into orbits with increasingly higher values of the orbit

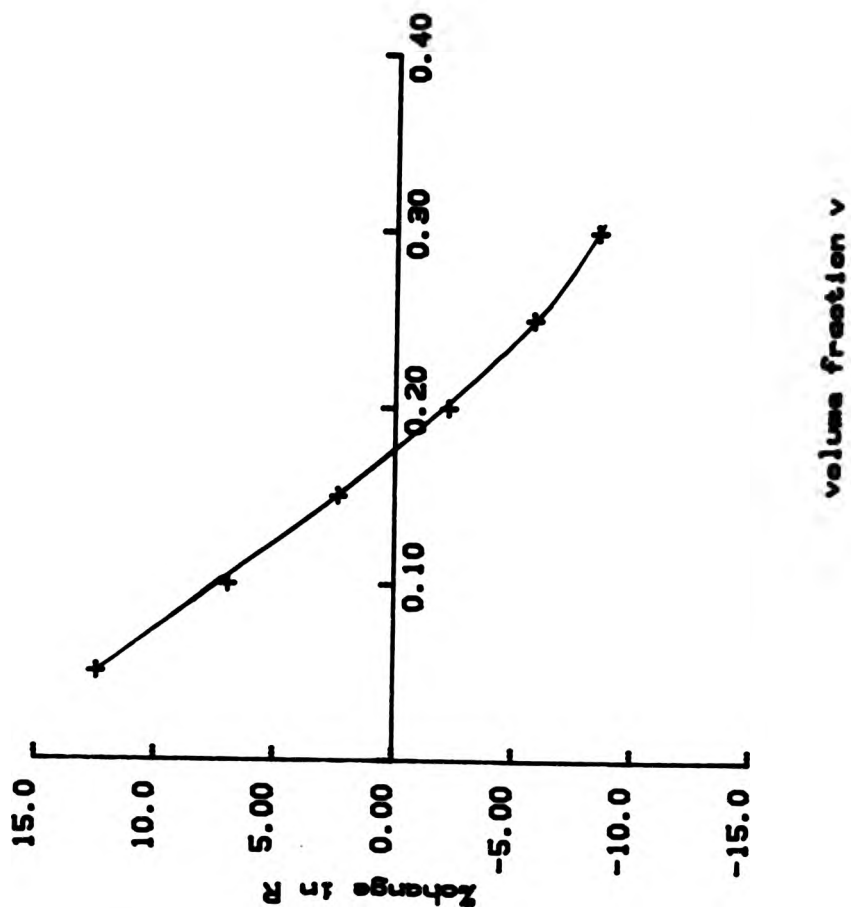


Figure 5.12 The percentage change in R as a function of volume fraction v for SPS

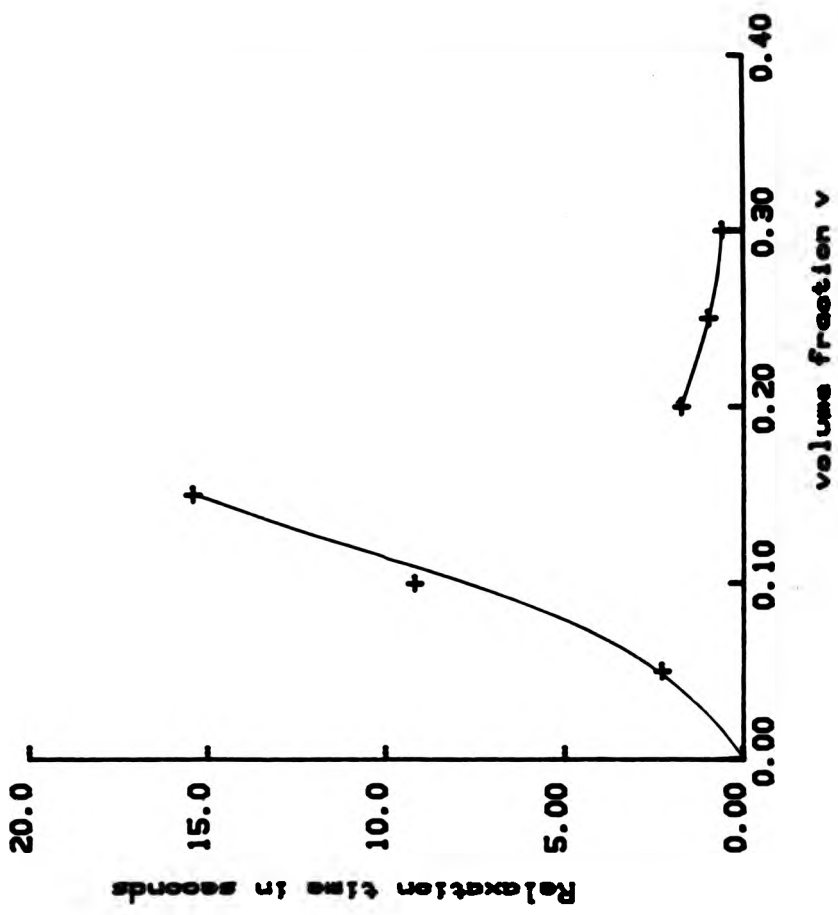


Figure 5.13 Relaxation time as a function of volume fraction  $v$  for SPS

constant C. Essentially a non-spherical particle in a shear field rotates with a non-uniform angular velocity and if acted upon by no other couples, spends most of its time with its longest dimension in the direction of the streamlines(16). The volume required by the particle for rotation suggests a critical volume fraction above which rotation will be impeded by the proximity of neighbouring particles.

The upper limit of the rotation volume will be the volume of a sphere with a diameter equal to the longest dimension of the particle. In the present case this will be the diameter of the disc face. This therefore defines a critical volume fraction,  $v_c$ , which is simply the ratio of the particle volume to the rotation volume.

In terms of the axis ratio,  $r_p$  for a thin disc *this gives*

$$v_c = 3/2 r_p \quad (5.3)$$

The axis ratio for kaolinite is taken as 0.1 from electron microscopy. The critical volume fraction is then given as 0.15.

This result shows excellent agreement with the data presented in figure 5.13.

Above this critical volume fraction the particles will be constrained to rotate in orbits requiring less volume, i.e. lower values of C. As the concentration increases beyond this critical value, C will become increasingly small tending to zero. At this value of the orbit constant the particles rotate in their own volume and when oriented in this way the particle normal is also normal to the flux direction. The minimum geometric area is in the incident

plane and the incident flux sees on average more disc edges than faces.

Relaxation times from both face-on orientation and edge-on orientation have previously been measured(50) in dilute kaolinite suspensions at a volume fraction of  $10^{-4}$ . They report that relaxation from face-on orientation is a factor of approximately six times slower than from edge-on orientation. It is seen that this result compares well with the relaxation times presented in figure 5.13.

Using a simple diffraction limit for the scattering cross-section in a single scattering experiment,

$$C(\theta) = (\cos^2\theta + p^2 \sin^2\theta) \quad (5.4)$$

it is possible to calculate the angular deviation necessary for the in-plane scattering cross-section to decay to  $1/e$  of its initial value for face-on orientation, or to rise to  $(1-1/e)$  of its initial value for edge-on orientation. Assuming that the relaxation time is proportional to this angular deviation, it is possible to calculate the ratio of relaxation times for face-on and edge-on orientation.

The normalised scattering cross-section  $C_N$  starting from face-on orientation is

$$C_N(\theta) = \frac{C(\theta) - C(\text{RANDOM})}{C(0) - C(\text{RANDOM})} \quad (5.5)$$

and starting from edge-on orientation

$$C_N(\theta) = \frac{C(\theta) - C(\text{RANDOM})}{C(90) - C(\text{RANDOM})} \quad (5.6)$$

For face-on orientation the required angle is given by

$$C_N(\theta) = C_N(0)/e \quad (5.7)$$

and for edge-on orientation

$$C_w(\theta) = C_w(90) (1 - 1/e) \quad (5.8)$$

Using this approach and the values for  $C(0)$ ,  $C(90)$  and  $C(\text{RANDOM})$  given in chapter 3.1, the relaxation time ratio obtained is 3.11 i.e. relaxation from face-on orientation is three times slower than edge-on relaxation which gives reasonable agreement with previous data[50] considering the simplistic model.

However the data presented here were obtained in a multiple scattering experiment. Using the same model but with the diffuse scattering cross-section  $C_w(\theta)$  derived in chapter 3.1 and the values for face-on, edge-on and random orientation i.e.  $C_w(0)$ ,  $C_w(90)$  and  $C_w(\text{RANDOM})$ , the relaxation time ratio is reduced to 2.4 for a multiple scattering system. This result indicates that more complex relaxation models are required in concentrated systems to take account of the effect of hydrodynamic and electrostatic inter-particle interactions.

The decrease in relaxation time above the critical volume fraction is thought to be due to the increase in elasticity produced by the energy of electrostatic repulsion when the particles are constrained to flow with their faces closer and parallel to each other.

## Chapter 6

### Conclusion

In this chapter some of the results from the experimental work are briefly summarised.

There exists, perhaps a hierarchy of scientific problems in colloid science. Most of the work reported seems to have been carried out on well characterised particulate systems e.g. mono-disperse spherical latex particles in stabilised suspensions. Work on more complex systems is left to the industries using colloids to carry out internally, and much of this work remains unpublished for commercial reasons.

Comparisons with results obtained by other workers using optical techniques is therefore limited to dilute dispersions under single scattering conditions. Theoretical comparisons are also limited because of the assumptions used developing the theories.

The Mie theory is strictly valid only for systems of spherical mono-disperse independent scatterers.

In the case of Jeffery's theory of particle orientation, low (creeping) shear and the absence of inter-particle forces and Brownian motion are the limiting assumptions. Theories describing the behaviour of a dispersion in an acoustic field are at present lacking. Optical theories relating to multiple scattering systems are, apart from the simplified analyses carried out in this work, unable to cope at present with boundaries (e.g. sample cells) and non-spherical particles in orienting fields.

In this work a simple empirical approach has been adopted. Using this approach it has been possible to develop simple

models which have, to varying degrees of success, characterised the data.

Here concentrated suspensions of non-spherical polydisperse particles have been studied, using an optical probe. Where necessary experimental systems have been designed to aid this investigation and finally it has been shown that optics is no longer limited to dilute systems.

Bearing this in mind it is then possible to claim a measure of success.

#### 6.1 Static S measurements

The variation of the scattering parameter  $S$  was determined as a function of particle size at a volume fraction of 0.01, the results obtained showed good agreement with the Mie theory, however due to the limitations of the transmittance technique, discussed in chapter two data at higher concentrations were not obtained. Attempts were made to repeat this experiment using the optical fibre reflectance cell these proved unsuccessful owing to errors due to settling at the higher particle size fractions. Settling was not apparent in the transmittance system over the sampling time because altering the path length produced a mixing effect and the optical input and detection axis was in the horizontal plane. Using the reflectance technique settling produced discontinuities in the value of  $R$  obtained as a function of path length.

The scattering parameter  $S$  was also measured as a function of the dispersion  $\text{pH}$ . It was found not to vary. In chapter two temporal and optical coherence is discussed in



some detail and it is concluded that great care must be taken in experimental design to ensure that the data obtained are meaningful. For example if thin samples are used in an experiment designed to monitor changes in opacity with flocculation, such that single scattering is dominant and a quasi-monochromatic light source e.g. a laser is used, the coherence length and the coherence area will be such that variations of opacity with the state of flocculation may indeed be detected. If in practice the material is used as an optically thick coating and is required to be opaque in diffuse light, then controlling flocculation will prove costly and ineffective.

Using the fibre optic reflectance cell the variation of  $S$  with concentration was measured. Despite the problems encountered in characterising the data theoretically it was found that  $S$  was a non-linear function of the concentration and the scattering power per particle decreased with concentration. This data gave excellent agreement when compared to the Mie theory using a concentration dependant relative refractive index. This result suggests that at higher concentrations  $S$  will maximise and thereafter decrease with increasing concentration in the absence of particle ordering at higher concentrations. This therefore highlights the danger of conducting experiments at scaled down concentrations and the usefulness of the multiple scattering experimental system.

Measurements of  $S$  as a function of pH were also made using the reflectance cell at a volume fraction of 0.2, although not reported in the main text, again within the

experimental error no change in S was observed.

### 6.3 Orientational phenomena

As discussed in chapter three it is well documented that orientation of non-spherical particles produces changes in the geometric and scattering cross-section in a single scattering experiment. This indicates the usefulness of single scattering techniques in monitoring spheroid eccentricity. The theory developed in chapter three although simplistic in its assumptions shows for the first time that this information content is retained, even in the worst case of completely isotropic flux, in a multiple scattering experimental system.

In chapters three, four and five, the ability of particles or flocs to orient in an applied field has been used to monitor flocculation at volume fractions upto 0.2.

In chapter four evidence for acoustic scattering was obtained indicating the use of frequency dependant ultrasonic scattering as an on-line mean particle sizer.

In chapter five the mode of orientation in shear flow is shown to provide information on particle interactions when competition for space limits rotation, allowing the particle axis ratio to be operationally defined.

- 1) G.H.Meeten.(ed.) "Optical Properties of Polymers"  
Elsevier, London, 1986
- 2) N.Wax., "Selected papers on noise and stochastic  
processes" New York 1954, Dover
- 3) J. Perrin., J. Phys. Rad. (7) 5, 497, 1934
- 4) J. Gregory., J. COLL. INT. SCI. 105 357 1985
- 5) P. Kubelka, F.Munk., Z. Tech. Phys., 12, 593 1931
- 6) P. S. Mudgett, L. W. Richards., Appl. Opt., 10, 1485  
1971
- 7) A. Ishimaru., "Wave Propagation and Scattering in Random  
Media" Academic Press New York 1978
- 8) B. J. Brinkworth., J. Phys. D:Appl. Phys., 5, 476 1976
- 9) D. B. Judd, G. Wyszecchi., "Colour in Business, Science  
and Industry." Wiley, N. York. 1952
- 10) J. V. Champion, D. Downer, G. H. Meeten, S. A. Vaudrey,  
L. F. Gate., J. Chem. Soc. Far. II., 74, 843, 1978
- 11) P. J. Malden, R. E. Meads., Nature, 215, 844, 1967
- 12) J. H. Van. Vleck., Disc. Far. Soc., 26, 96, 1958
- 13) E. A. C. Follet., Soil. Sci., 16, 334, 1965
- 14) D. J. Greenland, J. M. Oades, T. W. Sharwin., Soil.  
Sci., 19, 123, 1968
- 15) D. A. Jefferson, M. J. Tricker, A. P. Winterbottom.,  
Clays and Clay Minerals. 23, 355, 1975
- 16) G. B. Jeffery., Proc. Roy. Soc., A102, 161, 1922
- 17) H. L. Goldsmith, S. G. Mason., "The Microrheology of  
dispersions" Pulp and Paper Research Inst. of Canada., 1965
- 18) L. G. Leal, E. J. Hinch., J. Fluid. Mech., 46, 685,  
1970

- 19) H. L. F. Helmholtz., Wied. Ann., 7, 337, 1879
- 20) G. Gouy., J. Phys., 9, 457, 1910
- 21) D. L. Chapman., Philos. Mag., 6, 475, 1913
- 22) B. V. Derjaguin, L. Landau., Acta. Physiochem. U.R.S.S. 14, 633, 1941
- 24) E. J. W. Verwey, J. Th. G. Overbeek., "Theory of stability of lyophobic colloids.", Elsevier, Amsterdam., 1948
- 25) D. H. Napper., "Polymeric Stabilisation of Colloidal Dispersions" Acad. Press. London, 1983
- 26) L. S. Ornstein, F. Zernicke., Proc. K. Ned. Akad. Wet., 17, 793, 1914
- 27) R. H. Ottewill, Ber. Bunsenges., Phys. Chem., 89, 517, 1985
- 28) J. E. Kline., TAPPI., 50, 12, 1967
- 29) H. van. Olphen., "Introduction to Colloid Chemistry" Wiley New York., 1965
- 30) R. F. Conley., Clay and Clay Minerals., 14, 17, 1966
- 31) H. van. Olphen., "Clay Colloid Chemistry" Wiley, New York., 1963
- 32) K. Norrish., Disc. Faraday Soc., 18, 120, 1954
- 33) Th. F. Tadros., Adv. Coll. Int. Sci., 12, 141, 1980
- 34) L. F. Gate., ECCI. Private Communication
- 35) A. Sommerhauser, D. L. Sussman, W. Stumm., Koll. Zeit., 225, 147, 1968
- 36) A. K. Killey, G. H. Meeten, M. Senior., J. Chem. Soc. Faraday II, 77, 587, 1981

- 37) J. V. Champion, G. H. Meeten, M. J. Senior., J. Chem. Soc. Faraday II Trans., 74, 1319, 1978
- 38) N. C. Wickramasinghe., "Light scattering functions for small particles", London., 1973
- 39) B. A. James, D. J. A. Williams., Rheol. Acta. 21, 176, 1982
- 40) M. Born, E. Wolf., "Principles of Optics" Oxford., 1980
- 41) S. Fitzwater, J. W. Hook. III., J. Coat. Tech. 57, 721, 1985
- 42) L. F. Gates., J. Opt. Soc. Am. 63, 312, 1973
- 43) B. R. Moon., Phd. Thesis., City of London Polytechnic C.N.A.A. 1978
- 44) D. J. A. Williams, K. P. Williams., Trans. J. Ceram. soc. 81, 78, 1982.
- 45) A.B. Wood., "A textbook of sound" London, 1941
- 46) R. J. Urick., J. Appl. Phys. 18, 983, 1947
- 47) G. G. Stokes., Trans. Camb. Phil. Soc. 8, 287, 1849
- 48) G. Kirchhoff., Ann. Phys. Lpz., 143, 177, 1868
- 49) K. M. Beazley., J. Coll. Int. Sci., 41, 105, 1972
- 50) J. V. Champion, G. H. Meeten, B. R. Moon., J. Chem. Soc. Faraday Trans II., 75, 767, 1979
- 51) J. Gregory., Roy. Soc. Chem. Summer school "solid liquid dispersions" (Ed Th. F. Tadros) Acad. Press 1987

THE BRITISH LIBRARY DOCUMENT SUPPLY CENTRE

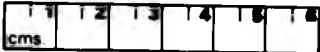
TITLE ..... OPTICAL PROPERTIES OF CONCENTRATED DISPERSIONS

AUTHOR ..... PETER J MOLLOY

INSTITUTION  
and DATE ..... CITY OF LONDON POLYTECHNIC  
1986

Attention is drawn to the fact that the copyright of this thesis rests with its author.

This copy of the thesis has been supplied on condition that anyone who consults it is understood to recognise that its copyright rests with its author and that no information derived from it may be published without the author's prior written consent.

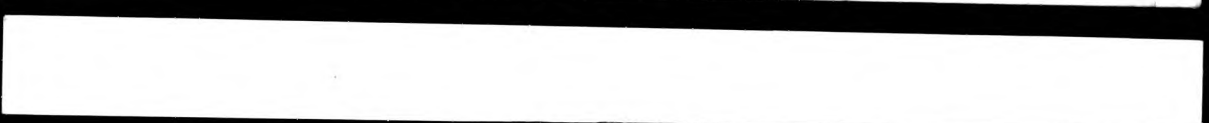


THE BRITISH LIBRARY  
DOCUMENT SUPPLY CENTRE  
Boston Spa, Wetherby  
West Yorkshire  
United Kingdom

REDUCTION X ..... 21



**DX**



<b>8</b>	<b>5</b>	<b>6</b>	<b>6</b>	<b>3</b>
----------	----------	----------	----------	----------

